AD-A089 833 SCIENCE APPLICATIONS INC BOULDER CO PLASMA RESEARCH INST F/G 20/5
SELF-CONSISTENT VLASOV DESCRIPTION OF THE FREE ELECTRON LASER I--ETC(U)
JAN 80 R C DAVIDSON, H S UHM N00014-79-C-0555
UNCLASSIFIED SAI-254-80-475-LJ NL

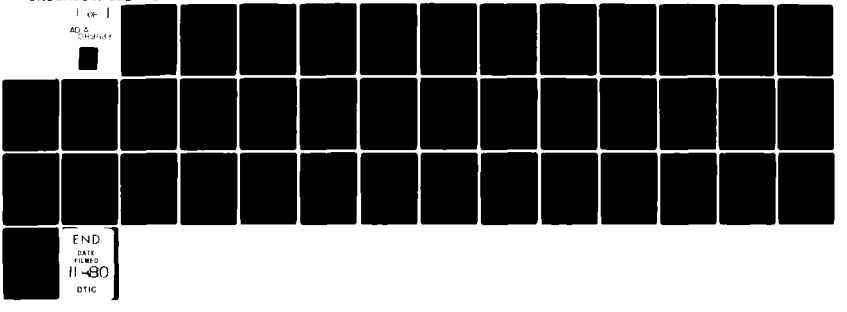

END
DATE FILMED
11-80
DTIC

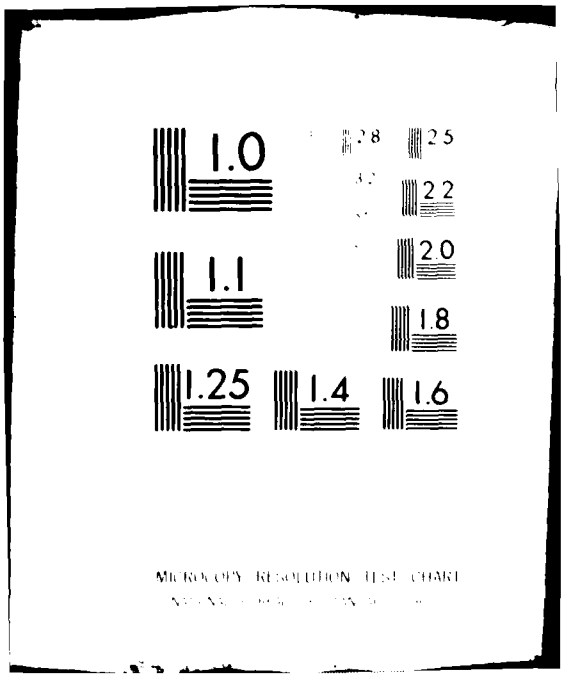
1.0
1.1
1.25
1.4
1.6
2.0
1.8
2.2
2.5
2.8
MICROCOPY RESOLUTION TEST CHART

AD A089833

REPORT NUMBER
SAI-254-80-475-LJ,
PRI-9

LEVEL II

SELF-CONSISTENT VLASOV DESCRIPTION OF THE FREE ELECTRON LASER INSTABILITY*

RONALD C. DAVIDSON AND HAN S. UHM

JAN 1980

DTIC
ELECTE
OCT 2 1980
S C

Reproduction in whole or in part is permitted for any purpose of the United States Government.

*Work supported by Office of Naval Research, Contract No: N00014-79-C-0555

SCIENCE APPLICATIONS INCORPORATED
PLASMA RESEARCH INSTITUTE
BOULDER, COLORADO

DDC FILE COPY

80 10 1 016

unclassified

SECURITY CLASSIFICATION OF THIS PAGE (When Data Entered)

REPORT DOCUMENTATION PAGE	READ INSTRUCTIONS BEFORE COMPLETING FORM
1. REPORT NUMBER: SAI-254-80-475-LJ ✓ AD-A089833	3. RECIPIENT'S CATALOG NUMBER
4. TITLE (and Subtitle): SELF-CONSISTENT VLASOV DESCRIPTION OF THE FREE ELECTRON LASER INSTABILITY	5. TYPE OF REPORT & PERIOD COVERED: Technical Report
	6. PERFORMING ORG. REPORT NUMBER: PRI-9 ✓
7. AUTHOR(s): Ronald C. Davidson* and Han S. Uhm** *Plasma Fusion Ctr., MIT **Naval Surface Weapons Ctr., Silver Springs, MD	8. CONTRACT OR GRANT NUMBER(s): N000-14-79-C-0555 ✓
9. PERFORMING ORGANIZATION NAME AND ADDRESS: Science Applications, Inc. Plasma Research Inst. ✓ 934 Pearl, Boulder, CO 80302	10. PROGRAM ELEMENT, PROJECT, TASK AREA & WORK UNIT NUMBERS
11. CONTROLLING OFFICE NAME AND ADDRESS: Office of Naval Research Physics Program Office Arlington, VA 22217	12. REPORT DATE: January, 1980
	13. NUMBER OF PAGES: 38
14. MONITORING AGENCY NAME & ADDRESS(if different from Controlling Office)	15. SECURITY CLASS. (of this report): Unclassified
	15a. DECLASSIFICATION/DOWNGRADING SCHEDULE

16. DISTRIBUTION STATEMENT (of this Report)

Approved for public release; distribution unlimited.

17. DISTRIBUTION STATEMENT (of the abstract entered in Block 20, if different from Report)

18. SUPPLEMENTARY NOTES

19. KEY WORDS (Continue on reverse side if necessary and identify by block number)

relativistic electron beam for free electron laser

20. ABSTRACT (Continue on reverse side if necessary and identify by block number)

A self-consistent description of the free electron laser instability is developed for a relativistic electron beam with uniform density propagating through a helical wiggler field $\underset{\sim}{B}^0 = -\hat{B}\cos k_0 z \hat{e}_x - \hat{B}\sin k_0 z \hat{e}_y$. The analysis is carried out for the class of solutions to the Vlasov-Maxwell equations described by $f_b(z,\underset{\sim}{p},t) = n_0\delta(P_x)\delta(P_y)G(z,p_z,t)$ where P_x and P_y are the exact

DD FORM 1 JAN 73 1473 EDITION OF 1 NOV 65 IS OBSOLETE S/N 0102-LF-014-6601

unclassified

SECURITY CLASSIFICATION OF THIS PAGE (When Data Entered)

canonical momenta invariants perpendicular to the beam propagation direction. The linearized Vlasov-Maxwell equations lead to an exact matrix dispersion relation which is valid for perturbations about general beam equilibrium $G_0(p_z)$ and includes coupling to arbitrary harmonic number (n) of the fundamental wiggler wavenumber k_0. No a priori restriction is made to low beam density (as measured by $\omega_p^2/c^2k_0^2$) or small wiggler amplitude (as measured by $\hat{\omega}_c/ck_0 = e\hat{B}/\bar{\gamma}mc^2k_0$). Moreover, no assumption is made that any off-diagonal elements in the matrix dispersion relation are negligibly small. A detailed numerical analysis of the exact dispersion relation is presented for the case of a cold electron beam described by $G_0(p_z) = \delta(p_z-p_0)$. It is shown that the instability bandwidth increases rapidly with increasing wiggler amplitude $\hat{\omega}_c/ck_0$. Moreover, except for very modest values of wiggler amplitude, it is shown that the growth rate calculated from an approximate version of the dispersion relation can be in substantial error for large values of $(k + nk_0)/k_0$. Preliminary estimates of the influence of beam thermal effects are also presented.

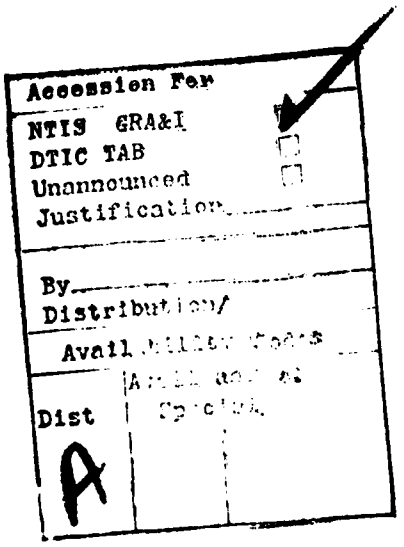

SELF-CONSISTENT VLASOV DESCRIPTION OF THE FREE ELECTRON LASER INSTABILITY

Ronald C. Davidson
Plasma Fusion Center
Massachusetts Institute of Technology
Cambridge, Mass., 02139

Han S. Uhm
Naval Surface Weapons Center
White Oak, Silver Spring, Md., 20910

A self-consistent description of the free electron laser instability is developed for a relativistic electron beam with uniform density propagating through a helical wiggler field $\underset{\sim}{B}^0 = -\hat{B}\cos k_0 z\hat{\underset{\sim}{e}}_x - \hat{B}\sin k_0 z\hat{\underset{\sim}{e}}_y$. The analysis is carried out for the class of solutions to the Vlasov-Maxwell equations described by $f_b(z,\underset{\sim}{p},t) = n_0\delta(P_x)\delta(P_y)G(z,p_z,t)$ where P_x and P_y are the exact canonical momenta invariants perpendicular to the beam propagation direction. The linearized Vlasov-Maxwell equations lead to an exact matrix dispersion relation which is valid for perturbations about general beam equilibrium $G_0(p_z)$ and includes coupling to arbitrary harmonic number (n) of the fundamental wiggler wavenumber k_0. No a priori restriction is made to low beam density (as measured by $\omega_p^2/c^2k_0^2$) or small wiggler amplitude (as measured by $\hat{\omega}_c/ck_0 = e\hat{B}/\bar{\gamma}mc^2k_0$). Moreover, no assumption is made that any off-diagonal elements in the matrix dispersion relation are negligibly small. A detailed numerical analysis of the exact dispersion relation is presented for the case of a cold electron beam described by $G_0(p_z) = \delta(p_z - p_0)$. It is shown that the instability bandwidth increases rapidly with increasing wiggler amplitude $\hat{\omega}_c/ck_0$. Moreover, except for very modest values of wiggler amplitude, it is shown that the growth rate calculated from an approximate version of the dispersion relation can be in substantial error for large values of $(k + nk_0)/k_0$. Preliminary estimates of the influence of beam thermal effects are also presented.

1. INTRODUCTION

In recent years there have been several theoretical[1-5] and experimental[6-8] investigations of the free electron laser which generates coherent electromagnetic radiation using an intense relativistic electron beam as an energy source. With few exceptions, theoretical studies of the free electron laser instability are based on highly simplified models which often neglect beam kinetic effects and coupling to higher harmonics of the fundamental wiggler wavenumber k_0, or make use of very idealized approximations in analyzing the matrix dispersion relation. The purpose of the present paper is to develop a fully self-consistent description of the free electron laser instability based on the Vlasov-Maxwell equations. The final matrix dispersion relation [Eq. (45)] includes all beam kinetic effects and coupling to arbitrary harmonic number (n) of the fundamental wiggler wavenumber k_0. Moreover, the final matrix dispersion relation [Eq. (45)] makes no a priori assumption that any off-diagonal elements are negligibly small.

The present analysis assumes a relativistic electron beam with uniform cross-section propagating in the z-direction through a helical wiggler field described by [Eq. (2)]

$$\underset{\sim}{B}^0 = -\hat{B}\cos k_0 z \hat{\underset{\sim}{e}}_x - \hat{B}\sin k_0 z \hat{\underset{\sim}{e}}_y$$

where $\hat{B}$ = const. is the field amplitude and $\lambda_0 = 2\pi/k_0$ is the wiggler wavelength. Moreover, we consider the class of exact solutions to the Vlasov-Maxwell equations described by [Eq. (12)][5]

$$f_b(z,\underset{\sim}{p},t) = n_0\delta(P_x)\delta(P_y)G(z,p_z,t),$$

where n_0 = const., P_x and P_y are the exact canonical momenta invariants [Eqs. (6) and (7)], and spatial variations are assumed to be one-dimensional. A detailed analysis of the linearized Vlasov-Maxwell equations (Secs. 2.B and 3.A) leads to the matrix dispersion relation [Eq. (45)]

$$D_n^L(\omega)\, D_{n+1}^T(\omega)\, D_{n-1}^T(\omega) = \frac{1}{2}\frac{\hat{\omega}_c^2}{c^2k_0^2}\left[D_{n+1}^T(\omega) + D_{n-1}^T(\omega)\right]$$

$$\times \left\{\left[\chi_n^{(1)}(\omega)\right]^2 - D_n^L(\omega)\left[\alpha_3\omega_p^2 + \chi_n^{(2)}(\omega)\right]\right\} ,$$

where $\hat{\omega}_c = e\hat{B}/\bar{\gamma}mc$ is the relativistic cyclotron frequency, $\omega_p^2 = 4\pi n_0 e^2/\bar{\gamma}m$ is the relativistic plasma frequency-squared, $\bar{\gamma}mc^2$ is the characteristic electron energy, α_3 is a constant of order unity [Eq.(43)], the susceptibilities $\chi_n^{(1)}(\omega)$ and $\chi_n^{(2)}(\omega)$ are defined in Eqs. (37) and (38), $D_n^L(\omega)$ is the longitudinal (electrostatic) dielectric function defined in Eq. (39), and $D_{n\pm1}^T(\omega)$ are the transverse (electromagnetic) dielectric functions defined in Eqs. (40) and (41). The striking feature of Eq. (45) is that the dispersion relation is valid for arbitrary harmonic number n. (No a priori assumption has been made that $n = \pm 1$). Moreover, the effective wavenumber variables that occur in the various factors in Eq. (45) are $k + nk_0$, $k + (n+1)k_0$ and $k + (n-1)k_0$. In addition, Eq. (45) describes stability behavior for perturbations about general beam equilibrium distribution $G_0(p_z)$, and no a priori restriction has been made to low beam density (as measured by $\omega_p/c^2k_0^2$) or small wiggler amplitude (as measured by $\hat{\omega}_c/ck_0$). Apart from the linearization assumption, no approximations have been made in deriving Eq. (45). For example, we have <u>not</u> assumed a priori that $D_n^L(\omega) \simeq 0$ and therefore neglected the corresponding term on the right-hand

side of Eq. (45). The latter point is very important. In Secs. 3.B and 3.C we present a detailed numerical analysis of the exact dispersion relation [Eq. (45)] for the case of a cold electron beam described by $G_0(p_z) = \delta(p_z - p_0)$. The exact stability results are then compared with the approximate results obtained from Eq. (45) by assuming at the outset that $D_n^L(\omega) \simeq 0$ and $D_{n-1}^T(\omega) \simeq 0$, which gives the reference dispersion relation [Eq. (46)]

$$D_n^L(\omega)D_{n-1}^T(\omega) = \frac{1}{2}\frac{\hat{\omega}_c^2}{c^2k_0^2}[\chi_n^{(1)}(\omega)]^2 .$$

For sufficiently large wiggler amplitude (as measured by $\hat{\omega}_c/ck_0$), it is shown in Sec. 3.C that the growth rate $\omega_i = \text{Im}\omega$ obtained from the reference dispersion relation [Eq.(46)] can be in substantial error for large values of $(k + nk_0)/k_0$.

For completeness, and to orient the reader, it is useful to summarize here the interaction wavenumbers and frequencies pertinent to the free electron laser instability.[9,10] We consider a cold electron beam (Secs. 3.B and 3.C) and look for simultaneous solutions to $D_n^L(\omega) = 0$ and $D_{n-1}^T(\omega) = 0$. Shown in Fig. 1 is a first-quadrant plot ($\omega > 0$ and $k + nk_0 > 0$) of

$$\omega = (k + nk_0)V_b \pm \omega_p/\bar{\gamma}$$

and

$$\omega = [c^2(k + nk_0 - k_0)^2 + \omega_p^2]^{1/2}$$

versus $k + nk_0$. Note that there are generally four intersection points. Solving the above equations simultaneously, the upshifted wavenumbers

(intersections with $k + nk_0 > k_0$) are given by

$$(k+nk_0)_u^{\pm} = \bar{\gamma}^2 k_0 \left[1+\beta_b \left(1 \pm 2 \frac{\omega_p}{ck_0} \frac{1}{\bar{\gamma}\beta_b} \right)^{1/2} \right] \pm \bar{\gamma}\beta_b \frac{\omega_p}{ck_0} k_0 ,$$

and the downshifted wavenumbers (intersections with $k+nk_0 < k_0$) are given by

$$(k+nk_0)_d^{\pm} = \bar{\gamma}^2 k_0 \left[1-\beta_b \left(1 \pm 2 \frac{\omega_p}{ck_0} \frac{1}{\bar{\gamma}\beta_b} \right)^{1/2} \right] \pm \bar{\gamma}\beta_b \frac{\omega_p}{ck_0} k_0 ,$$

where $\bar{\gamma} = (1 - \beta_b^2)^{-1/2}$ and $\beta_b = V_b/c$. In the limit of low beam density with $\omega_p^2/c^2k_0^2 \ll 1$, $\bar{\gamma}^2\beta_b^2$, the intersection wavenumbers can be approximated by

$$(k+nk_0)_u^{\pm} = (1+\beta_b)\bar{\gamma}^2 k_0 = k_0/(1-\beta_b),$$

and

$$(k+nk_0)_d^{\pm} = (1-\beta_b)\bar{\gamma}^2 k_0 = k_0/(1+\beta_b).$$

For sufficiently large $\bar{\gamma}$, the upshifted wavenumber $(k+nk_0)_u^{\pm} = (1+\beta_b)\bar{\gamma}^2 k_0$ can correspond to very short wavelengths and is the intersection region of interest for the free electron laser instability.[9,10] Depending on the value of beam density $(\omega_p^2/c^2k_0^2)$ and wiggler amplitude $(\hat{\omega}_c/ck_0)$, however, it is important to note that the dispersion relation (45) may also support instability in the long wavelength intersection region corresponding to $(k + nk_0)_d^{\pm}$. (See Sec. 3.C and Fig. 3).

2. THEORETICAL MODEL AND ASSUMPTIONS

A. General Theoretical Model

The present analysis assumes a relativistic electron beam with uniform cross section propagating in the z-direction. The beam density is assumed to be sufficiently small that equilibrium space charge effects are negligibly small with

$$\underset{\sim}{E}^0=0 \ . \tag{1}$$

Moreover, the electron beam propagates through a helical wiggler magnetic field described by [1,2,5]

$$\underset{\sim}{B}^0=-\hat{B}\cos k_0 z\hat{\underset{\sim}{e}}_x-\hat{B}\sin k_0 z\hat{\underset{\sim}{e}}_y \ , \tag{2}$$

where $\hat{B}$=const. is the field amplitude, $\lambda_0=2\pi/k_0$ is the wavelength, and $\hat{\underset{\sim}{e}}_x$ and $\hat{\underset{\sim}{e}}_y$ are unit Cartesian vectors in the plane perpendicular to the propagation direction. The vector potential associated with Eq. (2) is given by

$$\underset{\sim}{A}^0=(\hat{B}/k_0)\cos k_0 z\hat{\underset{\sim}{e}}_x+(\hat{B}/k_0)\sin k_0 z\hat{\underset{\sim}{e}}_y \ . \tag{3}$$

It is also assumed that the beam density and current are sufficiently small that the equilibrium self magnetic field can be neglected in comparison with $\underset{\sim}{B}^0$. [11]

We consider perturbations in which the spatial variations are one-dimensional in nature with $\partial/\partial x=0=\partial/\partial y$, and $\partial/\partial z$ generally non-zero. Introducing the perturbed potentials,

$$\delta\phi(z,t)$$

and

$$\delta\underset{\sim}{A}(\underset{\sim}{x},t)=\delta A_x(z,t)\hat{\underset{\sim}{e}}_x+\delta A_y(z,t)\hat{\underset{\sim}{e}}_y \ ,$$

the electromagnetic field perturbations $\delta\underset{\sim}{E}$ and $\delta\underset{\sim}{B}$ can be expressed in the Coulomb gauge as

$$\delta\underset{\sim}{E}(\underset{\sim}{x},t)=-\frac{\partial\delta\phi}{\partial z}(z,t)\hat{\underset{\sim}{e}}_z-\frac{1}{c}\frac{\partial}{\partial t}\delta A_x(z,t)\hat{\underset{\sim}{e}}_x-\frac{1}{c}\frac{\partial}{\partial t}\delta A_y(z,t)\hat{\underset{\sim}{e}}_y\ , \tag{4}$$

and

$$\delta\underset{\sim}{B}=-\frac{\partial}{\partial z}\delta A_y(z,t)\hat{\underset{\sim}{e}}_x+\frac{\partial}{\partial z}\delta A_x(z,t)\hat{\underset{\sim}{e}}_y\ , \tag{5}$$

where $\delta\underset{\sim}{E}=-\nabla\delta\phi-(1/c)(\partial/\partial t)\delta\underset{\sim}{A}$ and $\delta\underset{\sim}{B}=\nabla\times\delta\underset{\sim}{A}$. In the present geometry, there are two exact single-particle invariants in the combined equilibrium and perturbed field configuration. These are the canonical momenta, P_x and P_y, transverse to the beam propagation direction, i.e.,

$$P_x=p_x-\frac{e}{c}A_x^0(z)-\frac{e}{c}\delta A_x(z,t)=\text{const.}, \tag{6}$$

$$P_y=p_y-\frac{e}{c}A_y^0(z)-\frac{e}{c}\delta A_y(z,t)=\text{const.}, \tag{7}$$

where $A_x^0(z)=(\hat{B}/k_0)\cos k_0 z$ and $A_y^0(z)=(\hat{B}/k_0)\sin k_0 z$ [Eq. (3)], and p_x and p_y are the transverse mechanical momenta.

The potential perturbations $\delta\phi(z,t)$, $\delta A_x(z,t)$ and $\delta A_y(z,t)$ are determined self-consistently from the Maxwell equations

$$\left(\frac{1}{c^2}\frac{\partial^2}{\partial t^2}-\frac{\partial^2}{\partial z^2}\right)\delta A_x=-\frac{4\pi e}{c}\int d^3p\ v_x(f_b-f_b^0)\ , \tag{8}$$

$$\left(\frac{1}{c^2}\frac{\partial^2}{\partial t^2}-\frac{\partial^2}{\partial z^2}\right)\delta A_y=-\frac{4\pi e}{c}\int d^3p\ v_y(f_b-f_b^0)\ , \tag{9}$$

$$\frac{\partial^2}{\partial z^2}\delta\phi=4\pi e\int d^3p(f_b-f_b^0)\ , \tag{10}$$

where $f_b^0(z,\underset{\sim}{p})$ is the equilibrium ($\partial/\partial t=0$) beam distribution, and $f_b(z,\underset{\sim}{p},t)$ in general solves the nonlinear Vlasov equation

$$\left\{\frac{\partial}{\partial t}+v_z\frac{\partial}{\partial z}-e\left[\delta\underset{\sim}{E}+\frac{\underset{\sim}{v}\times(\underset{\sim}{B}^0+\delta\underset{\sim}{B})}{c}\right]\cdot\frac{\partial}{\partial\underset{\sim}{p}}\right\}f_b(z,\underset{\sim}{p},t)=0\ . \tag{11}$$

In Eqs. (8)-(11), the particle velocity $\underset{\sim}{v}$ and momentum $\underset{\sim}{p}$ are related by

$m\underset{\sim}{v}=\underset{\sim}{p}/(1+\underset{\sim}{p}^2/m^2c^2)^{1/2}$. Moreover, m is the electron rest mass, -e is the electron charge, and c is the speed of light in vacuo.

For present purposes, we examine the class of exact solutions to Eq. (11) of the form[5]

$$f_b(z,\underset{\sim}{p},t)=n_0\delta(P_x)\delta(P_y)G(z,p_z,t) \ , \tag{12}$$

where n_0=const., and P_x and P_y are the exact invariants defined in Eqs. (6) and (7). Note from Eq. (12) that the effective transverse motion of the beam electrons is "cold". Substituting Eq. (12) into Eq. (11) and making use of Eqs. (6) and (7), we find that Eq. (12) solves Eq. (11) exactly provided $G(z,p_z,t)$ evolves according to the one-dimensional Vlasov equation

$$\left\{\frac{\partial}{\partial t}+v_z\frac{\partial}{\partial z}-\frac{\partial}{\partial z}\hat{H}(z,t)\frac{\partial}{\partial p_z}\right\}G(z,p_z,t)=0 \ , \tag{13}$$

where $\hat{H}$ is defined by

$$\hat{H}(z,t)=\gamma_T mc^2-e\delta\phi(z,t) \ . \tag{14}$$

In Eq. (14),

$$\gamma_T mc^2\equiv[m^2c^4+c^2p_z^2+e^2(A_x^0+\delta A_x)^2+e^2(A_y^0+\delta A_y)^2]^{1/2} \ , \tag{15}$$

is the particle energy for $P_x=0=P_y$. Moreover, substituting Eq. (12) into Eqs. (8)-(11), the equations describing the nonlinear evolution of the potential perturbations can be expressed as

$$\left(\frac{1}{c^2}\frac{\partial^2}{\partial t^2}-\frac{\partial^2}{\partial z^2}\right)\delta A_x=-\frac{4\pi n_0e^2}{mc^2}\left[(A_x^0+\delta A_x)\int\frac{dp_z}{\gamma_T}G-A_x^0\int\frac{dp_z}{\gamma}G_0\right] \ , \tag{16}$$

$$\left(\frac{1}{c^2}\frac{\partial^2}{\partial t^2}-\frac{\partial^2}{\partial z^2}\right)\delta A_y=-\frac{4\pi n_0e^2}{mc^2}\left[(A_y^0+\delta A_y)\int\frac{dp_z}{\gamma_T}G-A_y^0\int\frac{dp_z}{\gamma}G_0\right] \ , \tag{17}$$

$$\frac{\partial^2}{\partial z^2}\delta\phi=-4\pi en_0\int dp_z[G-G_0] \ , \tag{18}$$

where $\gamma_T mc^2$ is defined in Eq. (15), $G_0(p_z)$ is the equilibrium ($\partial/\partial t = 0$) beam distribution, $G(z,p_z,t)$ solves the nonlinear Vlasov equation (13), and

$$\gamma mc^2=(m^2c^4+c^2p_z^2+e^2\hat{B}/k_0^2)^{1/2} , \tag{19}$$

is the energy in the absence of perturbations ($\delta A_x=0=\delta A_y$). In obtaining Eq. (19) from Eq. (15), use has been made of $(A_x^0)^2+(A_y^0)^2=\hat{B}^2/k_0^2=$const. [Eq. (3)].

Within the context of the present model, Eqs. (13) and (16)-(18) describe the exact nonlinear evolution of the system for perturbations about the general beam equilibrium $G_0(p_z)$. In this regard, we note from Eqs. (13) and (14) that the axial force F_z on an electron in the phase space (z,p_z) is given by

$$F_z=-\frac{\partial}{\partial z}\hat{H}=-\frac{e^2}{2\gamma_T mc^2}\frac{\partial}{\partial z}[2A_x^0\delta A_x+2A_y^0\delta A_y+(\delta A_x)^2+(\delta A_y)^2]+e\frac{\partial\delta\phi}{\partial z} . \tag{20}$$

That is, the effective ponderomotive potential is proportional to $2A_x^0\delta A_x+2A_y^0\delta A_y+(\delta A_x)^2+(\delta A_y)^2$.

B. Linearization Approximation

For purposes of the stability analysis, we now consider the linearized version of Eqs. (13) and (16)-(18). In this regard, it is useful to introduce the dimensionless potentials defined by

$$\delta\hat{\phi}=\frac{e\,\delta\phi}{\bar{\gamma}mc^2} , \tag{21}$$

$$\delta\hat{A}_\pm=\frac{e}{\bar{\gamma}mc^2}(\delta A_x\pm i\delta A_y) , \tag{22}$$

$$\hat{A}_\pm^0=\frac{e}{\bar{\gamma}mc^2}(A_x^0\pm iA_y^0)=\frac{\hat{\omega}_c}{ck_0}\exp(\pm ik_0z) . \tag{23}$$

In Eqs. (21)-(23), $\bar{\gamma}mc^2$=const. denotes the characteristic mean energy

of the electron beam, and

$$\hat{\omega}_c = \frac{e\hat{B}}{\bar{\gamma}mc} , \tag{24}$$

is the relativistic cyclotron frequency associated with the wiggler field amplitude $\hat{B}$. Making use of Eqs. (21)-(24), the perturbed force δF_z [Eq. (20)] and inverse relativistic mass factor γ_T^{-1} [Eq. (15)] can be approximated by

$$\delta F_z = -\bar{\gamma}mc^2 \left\{ \frac{1}{2} \frac{\hat{\omega}_c}{ck_0} \frac{\bar{\gamma}}{\gamma} \frac{\partial}{\partial z} \left[\exp(ik_0 z)\delta\hat{A}_- + \exp(-ik_0 z)\delta\hat{A}_+ \right] - \frac{\partial}{\partial z} \delta\hat{\phi} \right\} , \tag{25}$$

and

$$\frac{1}{\gamma_T} = \frac{1}{\gamma} - \frac{1}{2} \frac{\bar{\gamma}^{-2}}{\gamma^3} \frac{\hat{\omega}_c}{ck_0} \left[\exp(ik_0 z)\delta\hat{A}_- + \exp(-ik_0 z)\delta\hat{A}_+ \right] , \tag{26}$$

where $\gamma mc^2 = (m^2c^4 + c^2p_z^2 + e^2\hat{B}^2/k_0^2)^{1/2}$ [Eq. (19)]. Substituting Eqs. (25) and (26) into Eqs. (13) and (16)-(18), and combining Eqs. (16) and (17) to give equations for $\delta A_x \pm i\delta A_y$, the linearized equations for $\delta G(z,p_z,t)$, $\delta A_\pm(z,t)$ and $\delta\phi(z,t)$ can be expressed as

$$\left(\frac{\partial}{\partial t} + v_z \frac{\partial}{\partial z} \right) \delta G$$

$$= \bar{\gamma}mc^2 \left\{ \frac{1}{2} \frac{\hat{\omega}_c}{ck_0} \frac{\bar{\gamma}}{\gamma} \frac{\partial}{\partial z} \left[\exp(ik_0 z)\delta\hat{A}_- + \exp(-ik_0 z)\delta\hat{A}_+ \right] - \frac{\partial}{\partial z} \delta\hat{\phi} \right\} \frac{\partial}{\partial p_z} G_0(p_z), \tag{27}$$

$$\frac{\partial^2}{\partial z^2}\delta\phi = \frac{\omega_p^2}{c^2} \int dp_z \delta G , \tag{28}$$

$$\left(\frac{1}{c^2} \frac{\partial^2}{\partial t^2} - \frac{\partial^2}{\partial z^2} \right) \delta\hat{A}_+ = -\frac{\omega_p^2}{c^2} \left(\delta\hat{A}_+ \bar{\gamma} \int \frac{dp_z}{\gamma} G_0 \right.$$

$$+ \frac{\hat{\omega}_c}{ck_0} \exp(ik_0 z) \left\{ \bar{\gamma} \int dp_z \frac{\delta G}{\gamma} - \frac{1}{2} \frac{\hat{\omega}_c}{ck_0} \left[\exp(ik_0 z)\delta\hat{A}_- + \exp(-ik_0 z)\delta\hat{A}_+ \right] \right.$$

$$\left. \left. \times \bar{\gamma}^3 \int \frac{dp_z}{\gamma^3} G_0 \right\} \right), \tag{29}$$

$$\left(\frac{1}{c^2}\frac{\partial^2}{\partial t^2} - \frac{\partial^2}{\partial z^2}\right)\delta\hat{A}_- = -\frac{\omega_p^2}{c^2}\left(\delta\hat{A}_-\bar{\gamma}\int\frac{dp_z}{\gamma}G_0\right.$$

$$\left. + \frac{\hat{\omega}_c}{ck_0}\exp(-ik_0z)\left\{\bar{\gamma}\int dp_z\frac{\delta G}{\gamma} - \frac{1}{2}\frac{\hat{\omega}_c}{ck_0}\left[\exp(ik_0z)\delta\hat{A}_- + \exp(-ik_0z)\delta\hat{A}_+\right]\bar{\gamma}^3\int\frac{dp_z}{\gamma^3}G_0\right\}\right). \tag{30}$$

In Eqs. (28)-(30),

$$\omega_p^2 = \frac{4\pi n_0 e^2}{\bar{\gamma}m}\ , \tag{31}$$

is the relativistic plasma frequency-squared, and $\delta\hat{\phi}$, $\delta\hat{A}_\pm$ and $\hat{\omega}_c$ are defined in Eqs. (21), (22), and (24). In the limit of zero wiggler amplitude ($\hat{\omega}_c \to 0$), we note that Eqs. (27)-(30) give the usual uncoupled electromagnetic and electrostatic dispersion relations for perturbations about a one-dimensional relativistic plasma equilibrium.

3. STABILITY PROPERTIES

A. General Dispersion Relation

For the equilibrium configuration considered here, the electrons are constrained to move on surfaces with $P_x^0=p_x-(e/c)A_x^0=0=p_y-(e/c)A_y^0=P_y^0$ and $\gamma mc^2=(m^2c^4+c^2p_z^2+\hat{B}^2/k_0^2)^{1/2}=\text{const}$. This implies that the axial momentum p_z is a constant in the equilibrium field configuration. Moreover, the corresponding electron trajectory that passes through (z,p_z) at time $t'=t$ is given by

$$z'=z+\frac{p_z}{\gamma m}(t'-t) \ , \qquad p_z'=p_z, \tag{32}$$

where $p_z/\gamma m=v_z$ is the axial velocity.

Without loss of generality we expand the field perturbations in Eqs. (27)-(30) according to

$$\begin{aligned} \delta\hat{\phi}&=\sum_n \phi_n \exp[i(k+nk_0)z-i\omega t] \ , \\ \exp(ik_0z)\delta\hat{A}_-&=\sum_n A_{n-1}^- \exp[i(k+nk_0)z-i\omega t] \ , \\ \exp(-ik_0z)\delta\hat{A}_+&=\sum_n A_{n+1}^+ \exp[i(k+nk_0)z-i\omega t] \ , \end{aligned} \tag{33}$$

where $\lambda_0=2\pi/k_0$ is the periodicity length of the wiggler field. Here we assume that k is real and $\text{Im}\omega > 0$, corresponding to temporal growth. A completely parallel treatment can be developed for spatially growing perturbations ($\text{Im}k < 0$) and real oscillation frequency ω. Substituting Eq. (33) into Eq. (27) and integrating along characteristics, we obtain for the perturbed distribution function $\delta G(z,p_z,t)$

$$\delta G=\bar{\gamma}mc^2\frac{\partial G_0}{\partial p_z}\sum_n i(k+nk_0)\exp[i(k+nk_0)z]$$

$$\times\left(\frac{1}{2}\frac{\hat{\omega}_c}{ck_0}\frac{\bar{\gamma}}{\gamma}(A^-_{n-1}+A^+_{n+1})-\phi_n\right) \tag{34}$$

$$\times\int_{-\infty}^{t}dt'\exp[i(k+nk_0)v_z(t'-t)-i\omega t'] \ .$$

Integrating with respect to t' in Eq. (34) with $\mathrm{Im}\omega > 0$ gives

$$\delta G=\bar{\gamma}mc^2\frac{\partial G_0}{\partial p_z}\sum_n\frac{(k+nk_0)}{\omega-(k+nk_0)v_z}\exp[i(k+nk_0)z-i\omega t]$$

$$\times\left(\phi_n-\frac{1}{2}\frac{\hat{\omega}_c}{ck_0}\frac{\bar{\gamma}}{\gamma}(A^-_{n-1}+A^+_{n+1})\right) \ , \tag{35}$$

where $v_z=p_z/\gamma m$ and $\gamma mc^2=(m^2c^4+c^2p_z^2+\hat{B}^2/k_0^2)^{1/2}$.

From Eqs. (28)-(30) for the field perturbations, it is evident that integrals of the form $\omega_p^2\int dp_z\,\delta G$ and $\omega_p^2\bar{\gamma}\int dp_z\,\delta G/\gamma$ are required. Therefore, comparing with Eq. (35), it is convenient to introduce the effective susceptibilities $\chi_n^{(j)}(\omega)$ defined by

$$\chi_n^{(0)}(\omega)=\bar{\gamma}mc^2\omega_p^2\int dp_z\,\frac{(k+nk_0)\partial G_0/\partial p_z}{\omega-(k+nk_0)v_z} \ , \tag{36}$$

$$\chi_n^{(1)}(\omega)=\bar{\gamma}mc^2\omega_p^2\bar{\gamma}\int\frac{dp_z}{\gamma}\,\frac{(k+nk_0)\partial G_0/\partial p_z}{\omega-(k+nk_0)v_z} \ . \tag{37}$$

$$\chi_n^{(2)}(\omega)=\bar{\gamma}mc^2\omega_p^2\bar{\gamma}^2\int\frac{dp_z}{\gamma^2}\,\frac{(k+nk_0)\partial G_0/\partial p_z}{\omega-(k+nk_0)v_z} \ . \tag{38}$$

For future notational convenience we also introduce the longitudinal and transverse dielectric functions defined by

$$D_n^L(\omega)=c^2(k+nk_0)^2+\chi_n^{(0)}(\omega) \ , \tag{39}$$

$$D_{n+1}^T(\omega)=\omega^2-c^2[k+(n+1)k_0]^2-\alpha_1\omega_p^2 \ , \tag{40}$$

$$D_{n-1}^T(\omega)=\omega^2-c^2[k+(n-1)k_0]^2-\alpha_1\omega_p^2 \ , \tag{41}$$

where

$$\alpha_1=\bar{\gamma}\int \frac{dp_z}{\gamma}\, G_0(p_z) \tag{42}$$

and

$$\alpha_3=\bar{\gamma}^3\int \frac{dp_z}{\gamma^3}\, G_0(p_z) \tag{43}$$

for future reference. Note that the constants α_1 and α_3 are of order unity whenever G_0 is strongly peaked around $\gamma=\bar{\gamma}$.

We substitute Eqs. (33) and (35) into the field equations (28)-(30) and make use of the definitions in Eqs. (36)-(43). After some straightforward algebra, we obtain the matrix equation relating A^+_{n+1}, A^-_{n-1}, and ϕ_n

$$\begin{pmatrix} D^T_{n+1}+\frac{1}{2}\frac{\hat{\omega}_c^2}{c^2k_0^2}(\alpha_3\omega_p^2+\chi_n^{(2)}) & \frac{1}{2}\frac{\hat{\omega}_c^2}{c^2k_0^2}(\alpha_3\omega_p^2+\chi_n^{(2)}) & -\frac{\hat{\omega}_c}{ck_0}\chi_n^{(1)} \\ \frac{1}{2}\frac{\hat{\omega}_c^2}{c^2k_0^2}(\alpha_3\omega_p^2+\chi_n^{(2)}) & D^T_{n-1}+\frac{1}{2}\frac{\hat{\omega}_c^2}{c^2k_0^2}(\alpha_3\omega_p^2+\chi_n^{(2)}) & -\frac{\hat{\omega}_c}{ck_0}\chi_n^{(1)} \\ -\frac{\hat{\omega}_c}{ck_0}\chi_n^{(1)} & -\frac{\hat{\omega}_c}{ck_0}\chi_n^{(1)} & 2D_n^L \end{pmatrix} \begin{pmatrix} A^+_{n+1} \\ A^-_{n-1} \\ \phi_n \end{pmatrix} = 0. \tag{44}$$

The condition for a nontrivial solution to Eq. (44) is that the determinant of the matrix vanish. This gives the dispersion relation

$$\begin{aligned} D_n^L(\omega)D^T_{n+1}(\omega)D^T_{n-1}(\omega) = \frac{1}{2}\frac{\hat{\omega}_c^2}{c^2k_0^2}\,[D^T_{n+1}(\omega)+D^T_{n-1}(\omega)] \\ \times\{[\chi_n^{(1)}(\omega)]^2-D_n^L(\omega)[\alpha_3\omega_p^2+\chi_n^{(2)}(\omega)]\}\ , \end{aligned} \tag{45}$$

which determines the complex eigenfrequency ω in terms of $k+nk_0$, k_0, ω_p^2, and $\hat{\omega}_c^2/c^2k_0^2$.

The striking feature of Eq. (45) is that it is valid for arbitrary harmonic number n. (No a priori assumption has been made that $n=\pm1$.) Moreover, the effective wavenumber variable $k'=k+nk_0$ occurs in every factor in Eq. (45). In addition, Eq. (45) describes stability behavior

for general equilibrium distribution $G_0(p_z)$, and no a priori restriction has been made to low beam density (as measured by $\omega_p^2/c^2k_0^2$) or small wiggler amplitude (as measured by $\hat{\omega}_c/ck_0$). Since Eq. (45) contains no approximations apart from the linearization approximation, we refer to Eq. (45) as the full dispersion relation (FDR).

In circumstances where the beam density is low and the wiggler amplitude is very small, Eq. (45) supports solutions near $D_n^L(\omega)=0$, $D_{n+1}^T(\omega)=0$ and $D_{n-1}^T(\omega)=0$. In this case, it is instructive to simplify Eq. (45) near the simultaneous zeroes of $D_n^L(\omega)=0$ and $D_{n-1}^T(\omega)=0$. (Here we assume $D_{n+1}^T\neq 0$.) Equation (45) then reduces to the simplified approximate form

$$D_n^L(\omega)D_{n-1}^T(\omega)=\frac{1}{2}\frac{\hat{\omega}_c^2}{c^2k_0^2}\left[\chi_n^{(1)}(\omega)\right]^2 . \tag{46}$$

In the subsequent analysis, we refer to Eq. (46) as the reference dispersion relation (RDR).

B. Dispersion Relation for a Cold Electron Beam

As a first application, we consider the dispersion relation (45) for the case of a cold beam equilibrium described by

$$G_0(p_z)=\delta(p_z-p_0) , \tag{47}$$

where p_0 is related to the mean energy $\bar{\gamma}mc^2$ by

$$\bar{\gamma}mc^2=(m^2c^4+c^2p_0^2+e^2\hat{B}^2/k_0^2)^{1/2} . \tag{48}$$

It it straightforward to show from Eqs. (47) and (48) that $\int dp_z \gamma^n G_0(p_z)=\bar{\gamma}^n$ so that

$$\alpha_1=\alpha_3=1 , \tag{49}$$

follows from Eqs. (42) and (43). Substituting Eq. (47) into Eqs. (36)-(41), the effective susceptibilities and dielectric functions for a

cold electron beam can be expressed as

$$\chi_n^{(0)}(\omega)=-c^2(k+nk_0)^2\,\frac{\omega_p^2/\bar{\gamma}^2}{[\omega-(k+nk_0)V_b]^2}\,, \tag{50}$$

$$\chi_n^{(1)}(\omega)=c(k+nk_0)\omega_p^2\,\frac{[\omega\beta_b-c(k+nk_0)]}{[\omega-(k+nk_0)V_b]^2}\,, \tag{51}$$

$$\chi_n^{(2)}(\omega)=c(k+nk_0)\omega_p^2\,\frac{[2\omega\beta_b-c(k+nk_0)(1+\beta_b^2)]}{[\omega-(k+nk_0)V_b]^2}\,, \tag{52}$$

$$D_n^L(\omega)=c^2(k+nk_0)^2\left\{1-\frac{\omega_p^2/\bar{\gamma}^2}{[\omega-(k+nk_0)V_b]^2}\right\}\,, \tag{53}$$

$$D_{n+1}^T(\omega)=\omega^2-c^2[k+(n+1)k_0]^2-\omega_p^2\,, \tag{54}$$

$$D_{n-1}^T(\omega)=\omega^2-c^2[k+(n-1)k_0]^2-\omega_p^2\,. \tag{55}$$

In Eqs. (50)-(55), $V_b=p_0/\bar{\gamma}m$ is the beam velocity, and β_b is defined by $\beta_b=V_b/c$. Substituting Eqs. (50)-(55) into Eq. (45) and carefully ombining and simplifying terms on the right-hand side, the full dis- ersion relation (FDR) for the free electron laser instability can be expressed as

$$\begin{aligned}&\{[\omega-(k+nk_0)V_b]^2-\omega_p^2/\bar{\gamma}^2\}\{\omega^2-c^2[(k+nk_0)-k_0]^2-\omega_p^2\}\\&\quad\times\{\omega^2-c^2[(k+nk_0)+k_0]^2-\omega_p^2\}\\&=-\frac{\hat{\omega}_c^2}{c^2k_0^2}\,\omega_p^2[\omega^2-c^2(k+nk_0)^2-c^2k_0^2-\omega_p^2]\\&\quad\times\{[\omega-(k+nk_0)V_b]^2+2V_b(k+nk_0)[\omega-(k+nk_0)V_b]\\&\qquad-c^2(k+nk_0)^2/\bar{\gamma}^2-\omega_p^2\}\,.\end{aligned} \tag{56}$$

Note the exact cancellations that have occurred on the right-hand side of

Eq. (56). Making use of $\bar{\gamma}^{-2}=1-\beta_b^2$, the full dispersion relation (FDR) in Eq. (56) can be expressed in the equivalent form

$$\begin{aligned}&\{[\omega-(k+nk_0)V_b]^2-\omega_p^2/\bar{\gamma}^2\}\{\omega^2-c^2[(k+nk_0)-k_0]^2-\omega_p^2\}\\&\times\{\omega^2-c^2[(k+nk_0)+k_0]^2-\omega_p^2\}\\&=-\frac{\hat{\omega}_c^2}{c^2k_0^2}\,\omega_p^2[\omega^2-c^2(k+nk_0)^2-c^2k_0^2-\omega_p^2]\\&\times[\omega^2-c^2(k+nk_0)^2-\omega_p^2]\ .\end{aligned}\tag{57}$$

Moreover, substituting Eqs. (50), (51), (53), and (54) into Eq. (46), the reference dispersion relation (RDR), which is approximately valid for low beam density and very low wiggler amplitude, can be expressed as

$$\begin{aligned}&\{[\omega-(k+nk_0)V_b]^2-\omega_p^2/\bar{\gamma}^2\}\{\omega^2-c^2[(k+nk_0)-k_0]^2-\omega_p^2\}\\&=\frac{1}{2}\frac{\hat{\omega}_c^2}{c^2k_0^2}\,\omega_p^4\,\frac{[\omega\beta_b-c(k+nk_0)]^2}{[\omega-(k+nk_0)V_b]^2}\ .\end{aligned}\tag{58}$$

Approximating $[\omega-(k+nk_0)V_b]^2\simeq\omega_p^2/\bar{\gamma}^2$ in the denominator on the right-hand side of Eq. (57), the reference dispersion relation (RDR) becomes

$$\begin{aligned}&\{[\omega-(k+nk_0)V_b]^2-\omega_p^2/\bar{\gamma}^2\}\{\omega^2-c^2[(k+nk_0)-k_0]^2-\omega_p^2\}\\&=\frac{1}{2}\frac{\hat{\omega}_c^2}{c^2k_0^2}\,\omega_p^2\bar{\gamma}^{-2}[\omega\beta_b-c(k+nk_0)]^2\ .\end{aligned}\tag{59}$$

C. Numerical Analysis of Dispersion Relation

In this section, we summarize the results of numerical studies of the reference dispersion relation (59) and the full dispersion relation (57) for a broad range of dimensionless system parameters $\hat{\omega}_c/ck_0$, $\omega_p^2/c^2k_0^2$, and $\bar{\gamma}$.

Typical results are summarized in Fig. 2 for $\bar{\gamma}=2$ and moderate values of wiggler amplitude ($\hat{\omega}_c/ck_0=0.5$) and beam density ($\omega_p^2/c^2k_0^2=0.4$). For such large beam density and wiggler amplitude, we note from Fig. 2(a) that the growth rate $\omega_i=\text{Im}\omega$ obtained from the reference dispersion relation (59) can be in substantial error for large values of $(k+nk_0)/k_0$. This follows since the dashed curve in Fig. 2(a) [Eq. (59)] deviates significantly from the solid curve [Eq. (57)] for large values of $(k+nk_0)/k_0$. On the other hand, from Fig. 2(b), both the reference dispersion relation (59) and full dispersion relation (57) give very similar values of the real oscillation frequency $\omega_r=\text{Re}\omega$. Moreover, the oscillation frequency ω_r is linearly proportional to $(k+nk_0)$ over the entire range of unstable wavenumbers. We also note from Fig. 2(a) that the maximum growth assumes a relatively large value, $[\omega_i]_{max}\simeq 0.3\ ck_0$, for $(\hat{\omega}_c/ck_0,\ \omega_p^2/c^2k_0^2)=(0.5,\ 0.4)$.

To contrast with Fig. 2, we show in Fig. 3 a plot of normalized growth rate ω_i/ck_0 versus $(k+nk_0)/k_0$ for $\bar{\gamma}=2$, moderate beam density ($\omega_p^2/c^2k_0^2=0.4$), and <u>small</u> wiggler amplitude ($\hat{\omega}_c/ck_0=0.1$). In this case the reference dispersion relation (59) and full dispersion relation (57) give nearly identical growth rate curves. Note also from Fig. 3 that there are two unstable wavenumber bands [corresponding to two intersection regions of the ω versus $k+nk_0$ curves from $D_n^L(\omega)=0$ and $D_{n-1}^T(\omega)=0$] for $(\hat{\omega}_c/ck_0,\ \omega_p^2/c^2k_0^2)=(0.1,\ 0.4)$. Moreover, the maximum growth rate assumes a relatively small value, $[\omega_i]_{max}\simeq 0.06\ ck_0$, for the small value of wiggler amplitude chosen in Fig. 3.

Shown in Fig. 4, for $\bar{\gamma}=2$ and small wiggler amplitude ($\hat{\omega}_c/ck_0=0.1$), is a plot of normalized growth rate ω_i/ck_0 versus $(k+nk_0)/k_0$ [Eq. (57)] for several values of normalized beam density $\omega_p^2/c^2k_0^2$. An important feature of Fig. 4 is the fact that the instability bandwidth remains

reasonably narrow for $\omega_p^2/c^2k_0^2$ in the range $0.1 \leq \omega_p^2/c^2k_0^2 \leq 1$. This is in contrast to Fig. 5 where ω_i/ck_0 is plotted versus $(k+nk_0)/k_0$ [Eq. (57)] for $\bar{\gamma}=2$, moderate wiggler amplitude ($\hat{\omega}_c/ck_0=0.5$), and values of $\omega_p^2/c^2k_0^2$ identical to Fig. 4. The rapid increase of instability bandwidth with normalized wiggler amplitude $\hat{\omega}_c/ck_0$ is also evident from Fig. 6 where the growth rate is plotted for $\bar{\gamma}=2$, $\omega_p^2/c^2k_0^2=0.4$ and several values of $\hat{\omega}_c/ck_0$ [Eq. (57)].

We now examine the case where $\bar{\gamma}$ is large. Figures 7-11 show plots of normalized growth rate ω_i/ck_0 versus $(k+nk_0)/k_0$ for $\bar{\gamma}=50$ and a wide range of values of normalized wiggler amplitude $\hat{\omega}_c/ck_0$ and beam density $\omega_p^2/c^2k_0^2$. In all cases, we note from Figs. 7-11 that the instability bandwidth is large. This is in contrast with the low-$\bar{\gamma}$ case where the bandwidth is relatively narrow for small values of $\hat{\omega}_c/ck_0$ (Fig. 3). We also find (Figs. 7 and 8) that the growth rates determined from the reference dispersion relation (59) and the full dispersion relation (57) are different for both small wiggler amplitude (Fig. 8) and moderate wiggler amplitude (Fig. 7). This is in contrast with the low-$\bar{\gamma}$ case where the reference dispersion relation (59) gives a good estimate of the growth rate for small values of $\hat{\omega}_c/ck_0$ (Fig. 3). Comparing Figs. 4 and 9, for small wiggler amplitude ($\hat{\omega}_c/ck_0=0.1$), it is evident that the growth rate is considerably larger for large values of $\bar{\gamma}$. On the other hand, comparing Figs. 5 and 10, for moderate wiggler amplitude ($\hat{\omega}_c/ck_0=0.5$), the growth rate is only slightly larger for large values of $\bar{\gamma}$.

Finally, for $(k+nk_0)^2v_b^2 >> \omega_p^2/\bar{\gamma}^2$, we expect the strongest interaction between the longitudinal and transverse modes, $D_n^L(\omega)=0$ and $D_{n-1}^T(\omega)=0$, to occur for the critical value of wavenumber given in Sec. 1, i.e., for

$$(k+nk_0)_u \simeq (1+\beta_b)\bar{\gamma}^2k_0 \ . \qquad (60)$$

For $\beta_b \simeq 1$ and $\bar{\gamma}=50$, Eq. (60) gives $(k+nk_0)_s \simeq 5000\ k_0$. For $\bar{\gamma}=50$, we note from Figs. 7-11 that the maximum growth rate indeed occurs for $(k+nk_0)/k_0 \simeq 5000$.

D. Influence of Beam Thermal Effects on Stability Properties

The main purpose of this paper is to develop a stability formalism for general beam equilibrium distribution $G_0(p_z)$ (Secs. 2.A-3.A) and to study detailed stability properties for the case of a cold electron beam with $G_0(p_z)=\delta(p_z-p_0)$ (Secs. 3.B and 3.C). For completeness, however, in this section we make some preliminary estimates of the influence of beam thermal effects on stability behavior. As a simple example, we assume a beam equilibrium distribution of the form

$$G_0(p_z)= \frac{\Delta_0}{\pi} \frac{1}{(p_z-p_0)^2+\Delta_0^2} , \tag{61}$$

where Δ_0 is the characteristic momentum spread about the mean momentum p_0. We further assume that the momentum spread Δ_0 is small in comparison with the directed momentum p_0, i.e.,

$$\Delta_0 << p_0 . \tag{62}$$

Making use of Eqs. (36), (39), (61), and (62), the longitudinal dielectric function can be approximated by

$$D_n^L(\omega)=c^2(k+nk_0)^2\left(1- \frac{\omega_p^2/\bar{\gamma}^2}{[\omega-(k+nk_0)V_b+i|k+nk_0|\Delta_0/\bar{\gamma}^3m]^2}\right) , \tag{63}$$

for $\Delta_0 << p_0$. In Eq. (63), $\bar{\gamma}mc^2=(m^2c^4+c^2p_0^2+e^2\hat{B}^2/k_0^2)^{1/2}$ is the mean energy [Eq. (48)], and $V_b=p_0/\bar{\gamma}m$ is the directed beam velocity. We note from Eq. (63) that the fundamental longitudinal mode obtained from $D_n^L(\omega)=0$ is heavily Landau damped by thermal effects whenever

$$(k+nk_0)^2 \frac{\Delta_0^2}{\bar{\gamma}^6m^2} > \frac{\omega_p^2}{\bar{\gamma}^2} . \tag{64}$$

It is useful to express the effective momentum spread Δ_0 in terms of an equivalent energy spread $\Delta\gamma$. From $\gamma mc^2=(m^2c^4+c^2p_z^2+e^2\hat{B}^2/k_0^2)^{1/2}$, we estimate $\Delta\gamma=p_0\Delta_0/\bar{\gamma}m^2c^2$, or equivalently $\Delta\gamma/\bar{\gamma}=\beta_b\Delta_0/\bar{\gamma}mc$. Equation (64) can then be expressed as

$$c^2(k+nk_0)^2(\Delta\gamma/\bar{\gamma})^2>\beta_b^2\,\omega_p^2\bar{\gamma}^{-2}, \tag{65}$$

for $\Delta_0 \ll p_0$, or equivalently for $\Delta\gamma/\bar{\gamma} \ll \beta_b^2$. If we estimate the wavenumber of interest for the free electron laser instability by $(k+nk_0)=(1+\beta_b)\bar{\gamma}^2k_0$ [Eq. (60)], then Eq. (65) gives

$$(\Delta\gamma/\bar{\gamma})^2 > \frac{\beta_b^2}{(1+\beta_b)^2}\frac{1}{\bar{\gamma}^2}\frac{\omega_p^2}{c^2k_0^2}\,. \tag{66}$$

Equation (66) gives an estimate of the energy spread required for heavy Landau damping of the fundamental longitudinal mode obtained from $D_n^L(\omega)=0$. Whenever Eq. (66) is satisfied, the waves are heavily damped (linearly) and the free electron laser instability does not occur. Equation (66) constitutes a very stringent requirement on energy spread. For example, for $\bar{\gamma}=5$, $\beta_b=1$ and $\omega_p^2/c^2k_0^2=0.5$, Eq. (66) predicts stabilization for $(\Delta\gamma/\bar{\gamma})^2 > 5\times10^{-3}$, i.e., for a fractional energy spread $\Delta\gamma/\bar{\gamma}$ of about 7%.

From a practical point of view, for given values of $\bar{\gamma}$ and energy spread $\Delta\gamma$, the reverse of the inequality in Eq. (66) can be used to determine the range of normalized beam density $\omega_p^2/c^2k_0^2$ required for the free electron laser instability to occur, i.e.,

$$\frac{\omega_p^2}{c^2k_0^2} > \bar{\gamma}^2(\Delta\gamma/\bar{\gamma})^2\,\frac{(1+\beta_b)^2}{\beta_b^2}\,. \tag{67}$$

Whenever Eq. (67) is satisfied, it is important to note that the inequality in Eq. (65) will provide stabilization of the instability growth rate for sufficiently large values of wavenumber $(k+nk_0)$. This implies a natural tendency of beam thermal effects to limit the instability bandwidth, which should be contrasted with the cold-beam stability results in Sec. 3.C.

4. CONCLUSIONS

In this paper, we have developed a fully self-consistent description of the free electron laser instability based on the Vlasov-Maxwell equations. As summarized in Sec. 2, the present analysis assumes a relativistic electron beam with uniform cross section propagating through a helical wiggler field $\underset{\sim}{B}_0 = -\hat{B}\cos k_0 z\ \hat{e}_{\sim x} - \hat{B}\sin k_0 z\ \hat{e}_{\sim y}$ [Eq.(2)]. Moreover, we consider the class of exact solutions to the Vlasov-Maxwell equations described by $f_b(z,\underset{\sim}{p},t) = n_0\delta(P_x)\delta(P_y)G(z,p_z,t)$ [Eq.(12)]. A detailed analysis of the linearized Vlasov-Maxwell equations (Secs. 2.B and 3.A) leads to the exact matrix dispersion relation in Eq. (45). The striking feature of Eq. (45) is that the dispersion relation is valid for arbitrary harmonic number n. Moreover, Eq. (45) describes stability behavior for perturbations about general beam equilibrium distribution $G_0(p_z)$, and no a priori restriction has been made to low beam density (as measured by $\omega_p^2/c^2k_0^2$) or small wiggler amplitude (as measured by $\hat{\omega}_c/ck_0$). In Secs. 3.B and 3.C we present a detailed numerical analysis of the full dispersion relation [Eq.(57)] and the reference dispersion relation [Eq.(59)] for the case of a cold electron beam described by $G_0(p_z) = \delta(p_z - p_0)$. Except for very modest values of wiggler amplitude, it is shown in Sec. 3.C that the growth rate $\omega_i = \mathrm{Im}\omega$ obtained from the reference dispersion relation can be in substantial error for large values of $(k+nk_0)/k_0$. An important feature of the stability analysis in Sec. 3.C is the fact that the instability bandwidth increases rapidly with increasing $\hat{\omega}_c/ck_0$. Moreover, the instability bandwidth is considerably larger for large values of $\bar{\gamma}$ (Figs. 7 - 11) than for moderate values of $\bar{\gamma}$ (Figs. 2 - 6).

Finally, in Sec. 3.D, we have made preliminary estimates of the influence of beam thermal effects on stability behavior. In particular, assuming that $G_0(p_z)$ is given by the Lorentzian distribution in Eq.(61), it is found that waves with wavenumber $(k + nk_0) \simeq (1 + \beta_b)\bar{\gamma}^2 k_0$ are heavily Landau damped whenever the fractional energy spread $\Delta\gamma/\bar{\gamma}$ exceeds the rather modest value in Eq. (66).

ACKNOWLEDGEMENTS

This research was supported by the Office of Naval Research. The research by one of the authors (H.S.U.) was supported in part by the Independent Research Fund at the Naval Surface Weapons Center.

5. REFERENCES

1. T. Kwan and J.M. Dawson, Phys. Fluids 22, 1089 (1979).

2. T. Kwan, J.M. Dawson and A.T. Lin, Phys. Fluids 20, 581 (1977).

3. W.M. Manheimer and E. Ott, Phys. Fluids 17, 463 (1974).

4. P. Sprangle, J. Plasma Phys. 11, 299 (1974).

5. P. Sprangle and R.A. Smith, NRL Memorandum Report 4033 (1979); I. B. Bernstein and J. L. Hirshfield, Phys. Rev. A 20, 1661 (1979).

6. T.C. Marshall, S. Talmadge, and P. Efthimion, Appl. Phys. Lett. 31, 320 (1977).

7. D.A.G. Deacon, L.R. Elias, J.M.M. Madey, G.J. Ramian, H.A. Schwettman, and T.I. Smith, Phys. Rev. Lett. 38, 897 (1977).

8. L.R. Elias, W.M. Fairbank, J.M.J. Madey, H.A. Schwettman, and T.I. Smith, Phys. Rev. Lett. 36, 717 (1976).

9. H. Motz, J. Appl. Phys. 22, 527 (1950).

10. K. Landecker, Phys. Rev. 86, 852 (1951).

11. R.C. Davidson, Theory of Nonneutral Plasmas (Benjamin, New York, 1974).

FIGURE CAPTIONS

Fig. 1. Intersection of dispersion curves $D_n^L(\omega) = 0$ and $D_{n-1}^T(\omega) = 0$.

Fig. 2. Plot of normalized (a) growth rate ω_i/k_0c and (b) real oscillation frequency ω_r/k_0c versus normalized wavenumber $(k+nk_0)/k_0$ for $\gamma = 2$, $\hat{\omega}_c/ck_0 = 0.5$ and $\omega_p^2/c^2k_0^2 = 0.4$. Solid curves are obtained from full dispersion relation [Eq. (57)]. Dashed curves are obtained from reference dispersion relation [Eq. (59)].

Fig. 3. Plot of normalized growth rate ω_i/k_0c versus $(k+nk_0)/k_0$ for $\gamma = 2$, $\hat{\omega}_c/ck_0 = 0.1$ and $\omega_p^2/c^2k_0^2 = 0.4$ obtained from Eq. (57) (solid curves) and Eq. (59) (dashed curves).

Fig. 4. Plot of normalized growth rate ω_i/k_0c versus $(k+nk_0)/k_0$ obtained from Eq. (57) for $\gamma = 2$, $\hat{\omega}_c/ck_0 = 0.1$ and several values of $\omega_p^2/c^2k_0^2$.

Fig. 5. Plot of normalized growth rate ω_i/k_0c versus $(k+nk_0)/k_0$ obtained from Eq. (57) for $\gamma = 2$, $\hat{\omega}_c/ck_0 = 0.5$ and several values of $\hat{\omega}_p^2/c^2k_0^2$.

Fig. 6. Plot of normalized growth rate ω_i/k_0c versus $(k+nk_0)/k_0$ obtained from Eq. (57) for $\gamma = 2$, $\omega_p^2/c^2k_0^2 = 0.4$ and several values of $\hat{\omega}_c/ck_0$.

Fig. 7. Plot of normalized growth rate ω_i/k_0c versus $(k+nk_0)/k_0$ for $\gamma = 50$, $\hat{\omega}_c/ck_0 = 0.5$ and $\omega_p^2/c^2k_0^2 = 0.4$ obtained from Eq. (57) (solid curve) and Eq. (59) (dashed curve).

Fig. 8. Plot of normalized growth rate ω_i/k_0c versus $(k+nk_0)/k_0$ for $\gamma = 50$, $\hat{\omega}_c/ck_0 = 0.1$ and $\omega_p^2/c^2k_0^2 = 0.4$ obtained from Eq. (57) (solid curve) and Eq. (59) (dashed curve).

Fig. 9. Plot of normalized growth rate ω_i/k_0c versus $(k+nk_0)/k_0$ obtained from Eq. (57) for $\gamma = 50$, $\hat{\omega}_c/ck_0 = 0.1$ and several values of $\omega_p^2/c^2k_0^2$.

Fig. 10. Plot of normalized growth rate ω_i/k_0c versus $(k+nk_0)/k_0$ obtained from Eq. (57) for $\gamma = 50$, $\hat{\omega}_c/ck_0 = 0.5$ and several values of $\omega_p^2/c^2k_0^2$.

Fig. 11. Plot of normalized growth rate ω_i/k_0c versus $(k+nk_0)/k_0$ obtained from Eq. (57) for $\gamma = 50$, $\omega_p^2/c^2k_0^2 = 0.4$ and several values of $\hat{\omega}_c/ck_0$.

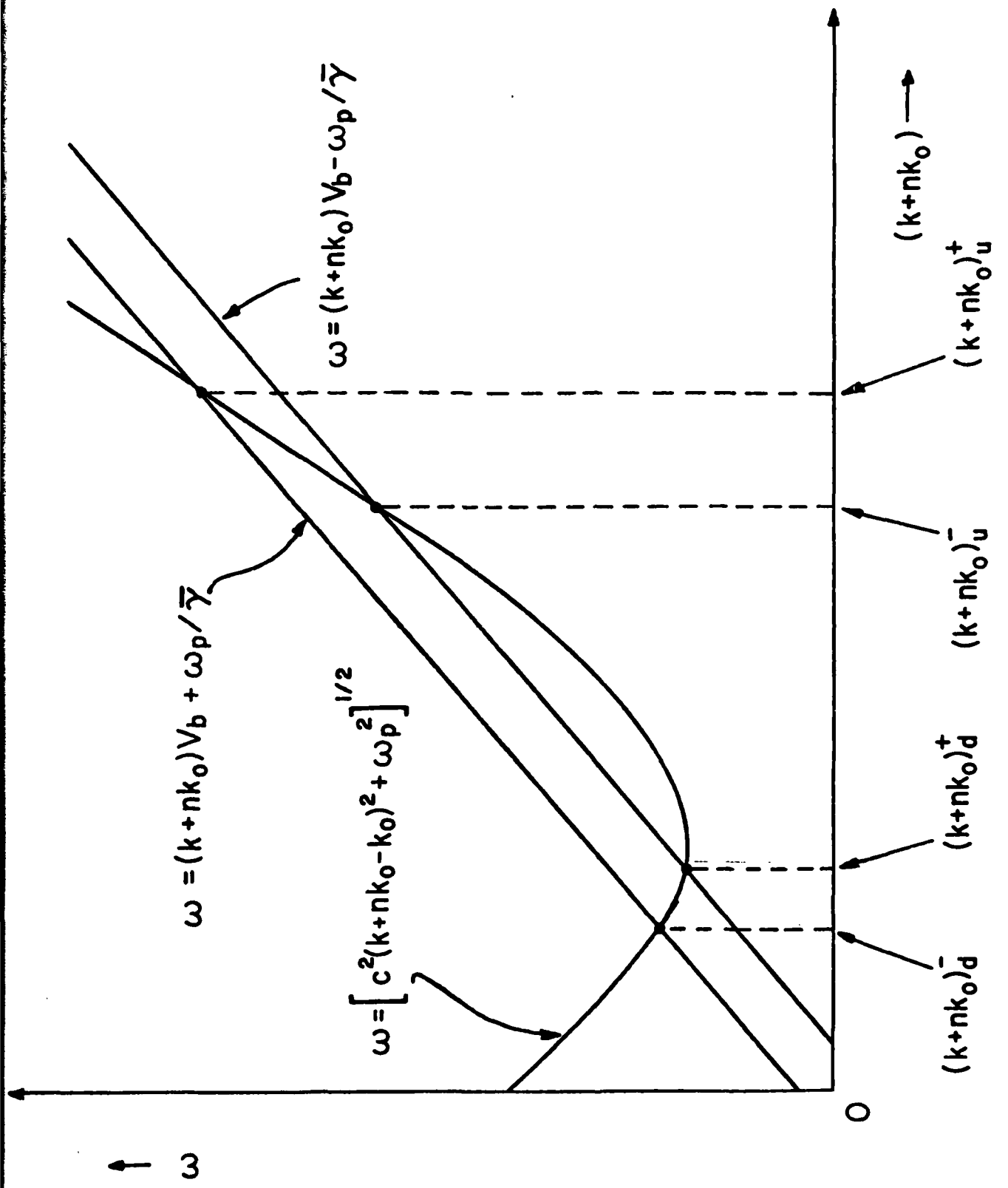
ω
(k+nk₀) ⟶
ω = (k+nk₀)V_b - ω_p/γ̄
ω = (k+nk₀)V_b + ω_p/γ̄
ω = [c²(k+nk₀-k₀)² + ω_p²]^1/2
(k+nk₀)⁺_u
(k+nk₀)⁻_u
(k+nk₀)⁺_d
(k+nk₀)⁻_d
0

Fig. 1

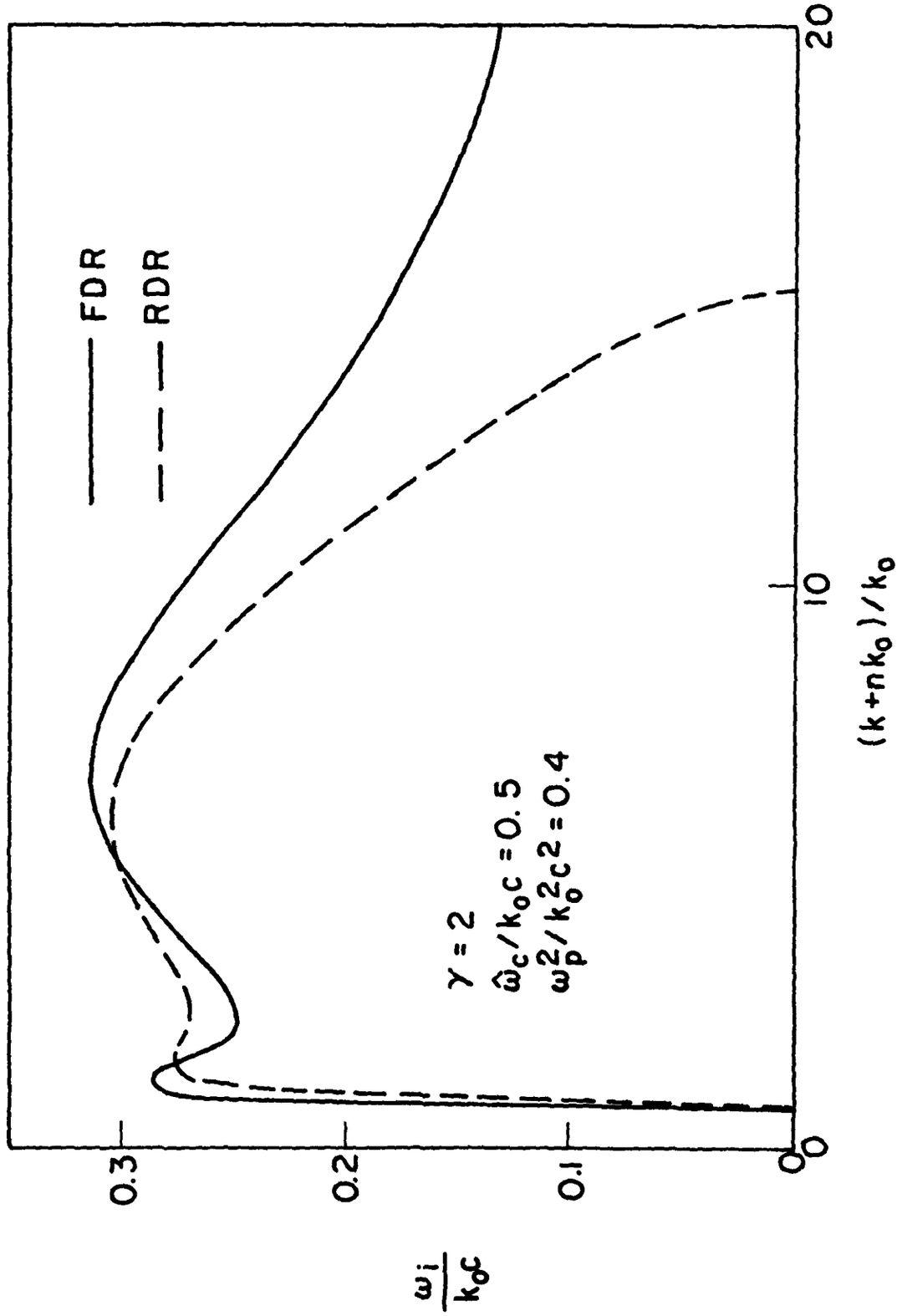
FDR
RDR
$\gamma = 2$
$\hat{\omega}_c/k_o c = 0.5$
$\omega_p^2/k_o^2 c^2 = 0.4$
0.3
0.2
0.1
0
10
20
$(k+nk_o)/k_o$
$\frac{\omega_i}{k_o c}$

Fig. 2(a)

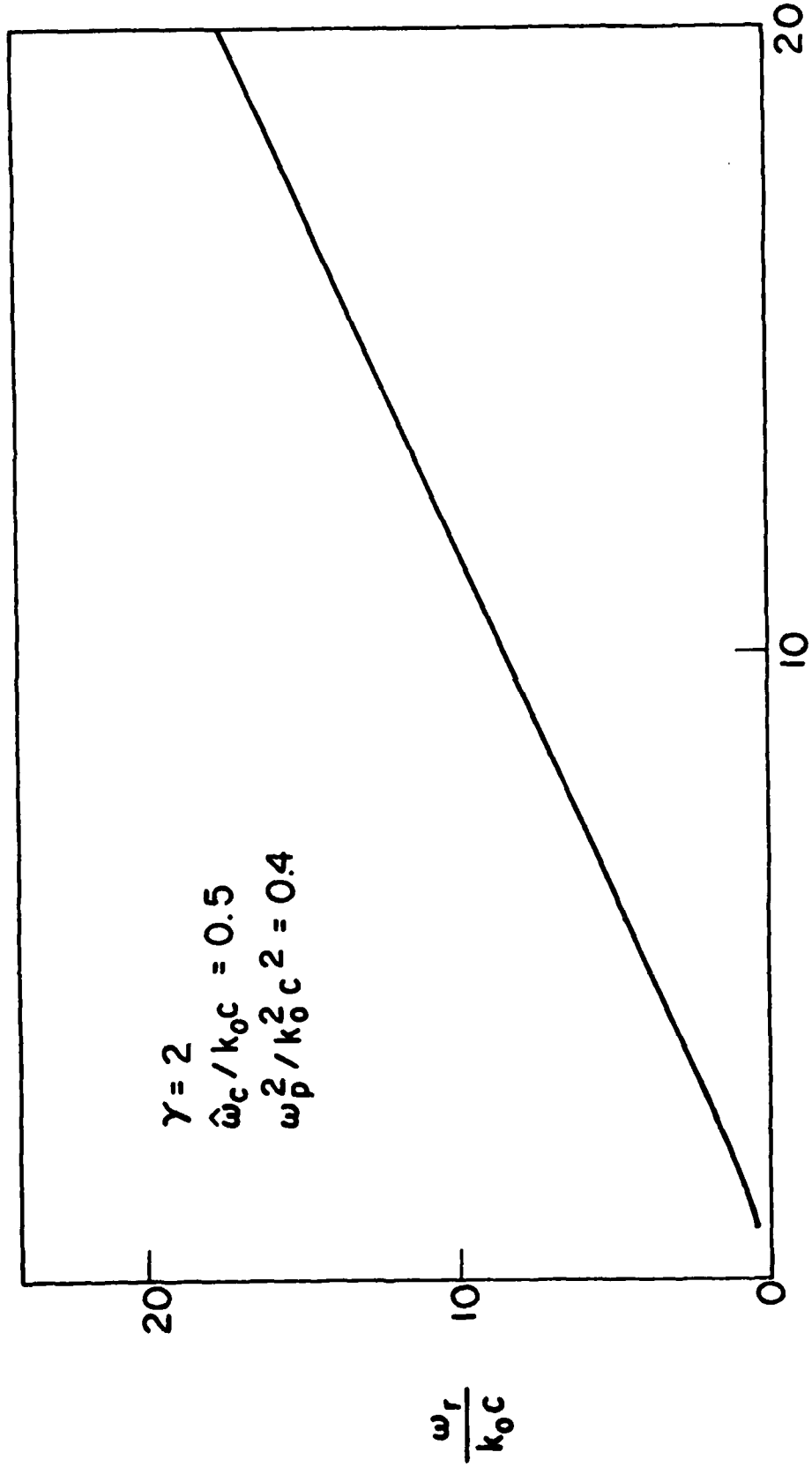
20
10
0
$\frac{\omega_r}{k_0 c}$
$\gamma = 2$
$\hat{\omega}_c / k_0 c = 0.5$
$\omega_p^2 / k_0^2 c^2 = 0.4$
10
20
$(k+n k_0)/k_0$

Fig. 2(b)

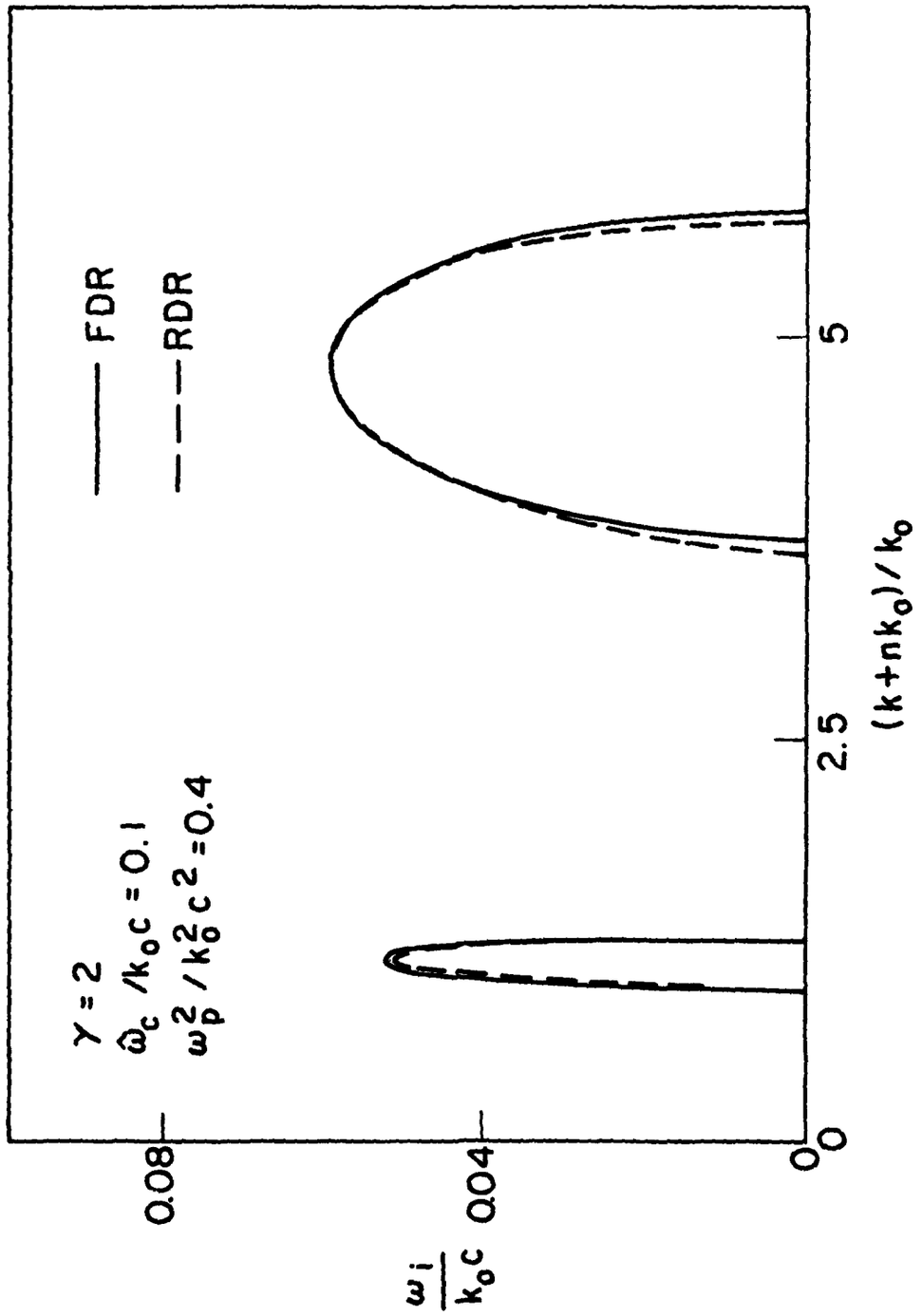

Fig. 3

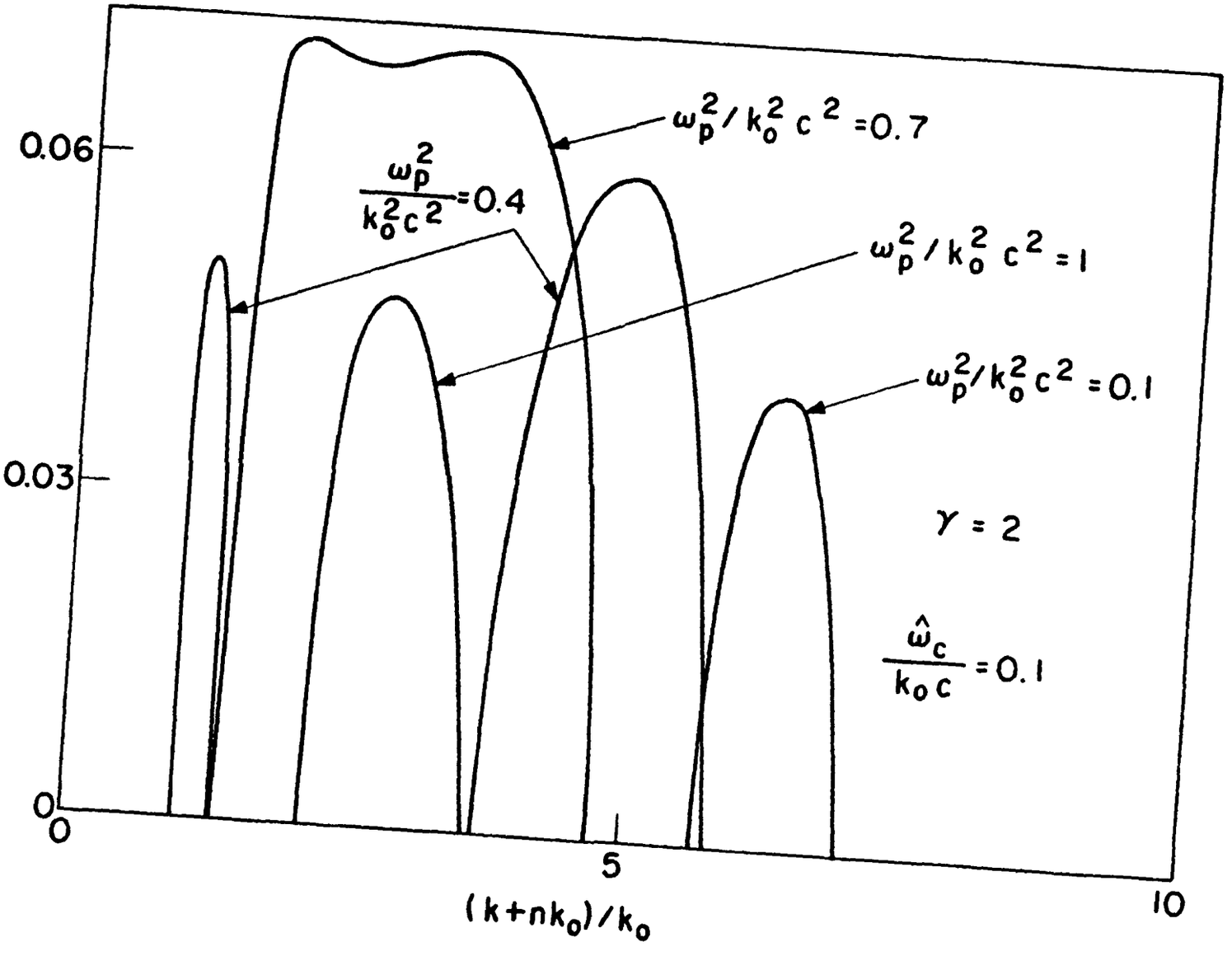
0.06
0.03
0
0
5
10
$\frac{\omega_i}{k_o c}$
$(k+nk_o)/k_o$
$\omega_p^2/k_o^2 c^2 = 0.7$
$\frac{\omega_p^2}{k_o^2 c^2} = 0.4$
$\omega_p^2/k_o^2 c^2 = 1$
$\omega_p^2/k_o^2 c^2 = 0.1$
$\gamma = 2$
$\frac{\hat{\omega}_c}{k_o c} = 0.1$

FIG. 4

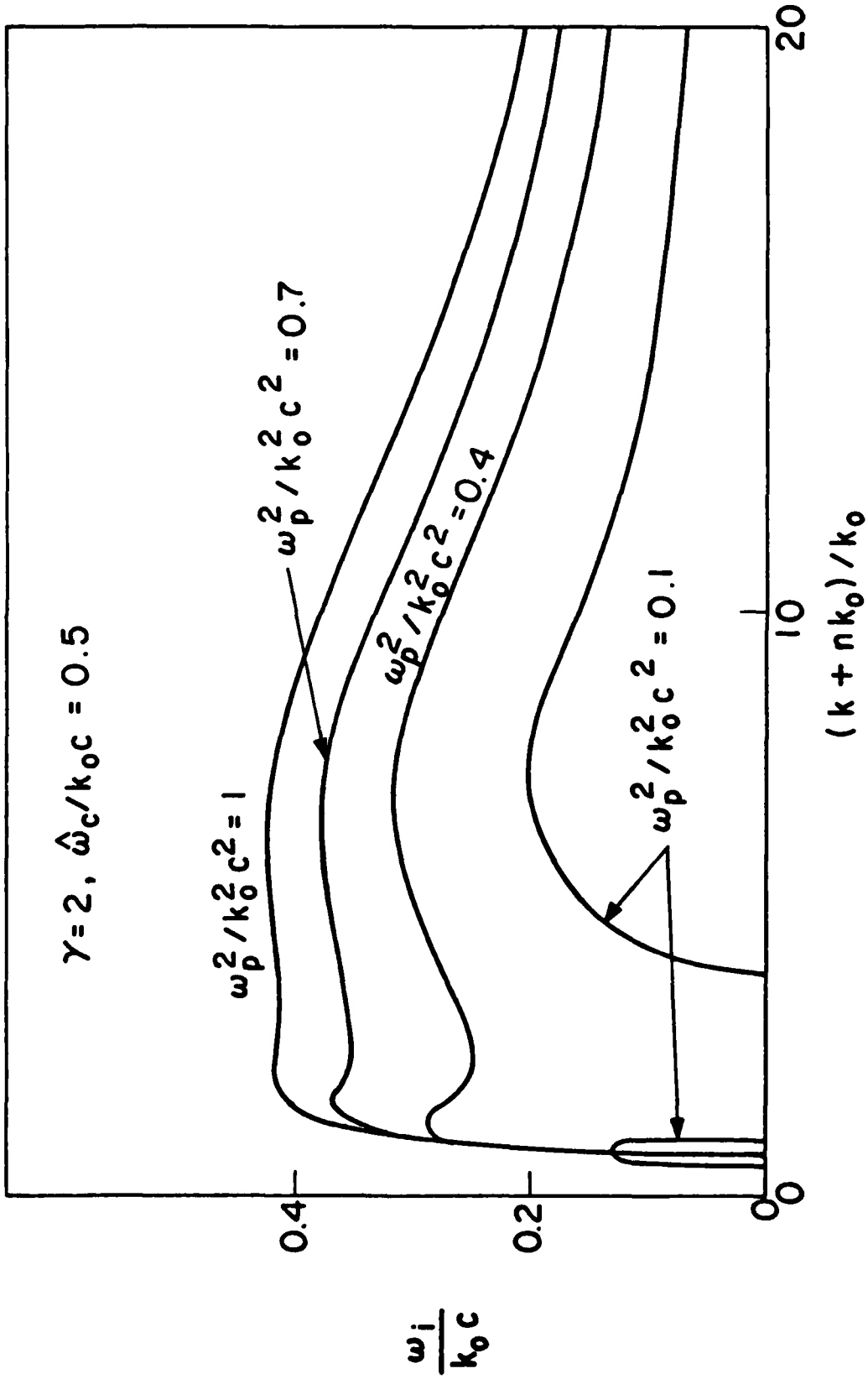
γ=2, ω̂c/k0c = 0.5
ω²p/k²0c² = 1
ω²p/k²0c² = 0.7
ω²p/k²0c² = 0.4
ω²p/k²0c² = 0.1
0.4
0.2
0
10
20
(k + nk0)/k0
ωi/k0c

Fig. 5

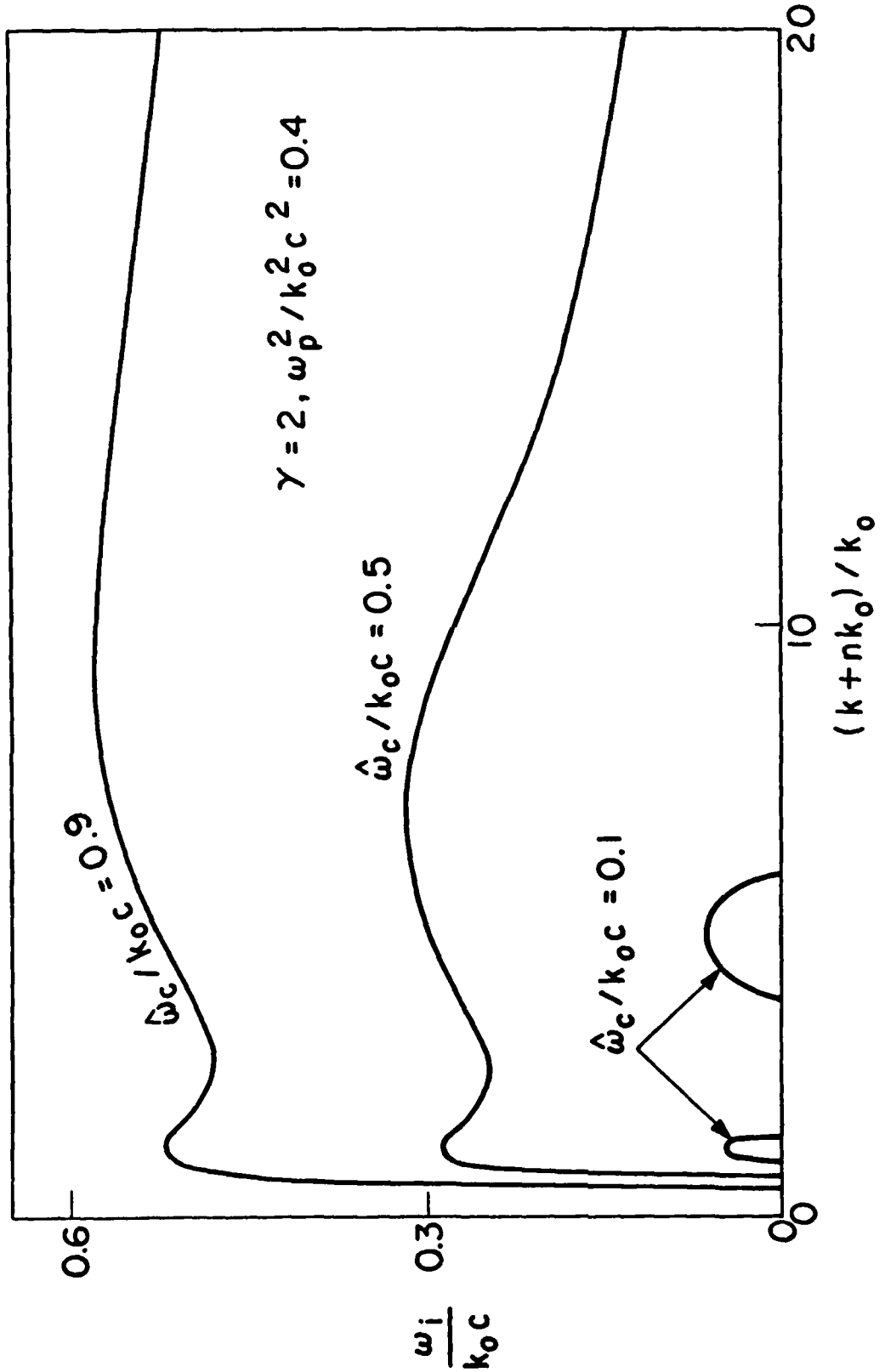
$\frac{\omega_i}{k_o c}$
0.6
0.3
0
10
20
$(k+nk_o)/k_o$
$\hat{\omega}_c/k_o c = 0.9$
$\hat{\omega}_c/k_o c = 0.5$
$\hat{\omega}_c/k_o c = 0.1$
$\gamma = 2, \omega_p^2/k_o^2 c^2 = 0.4$

Fig. 6

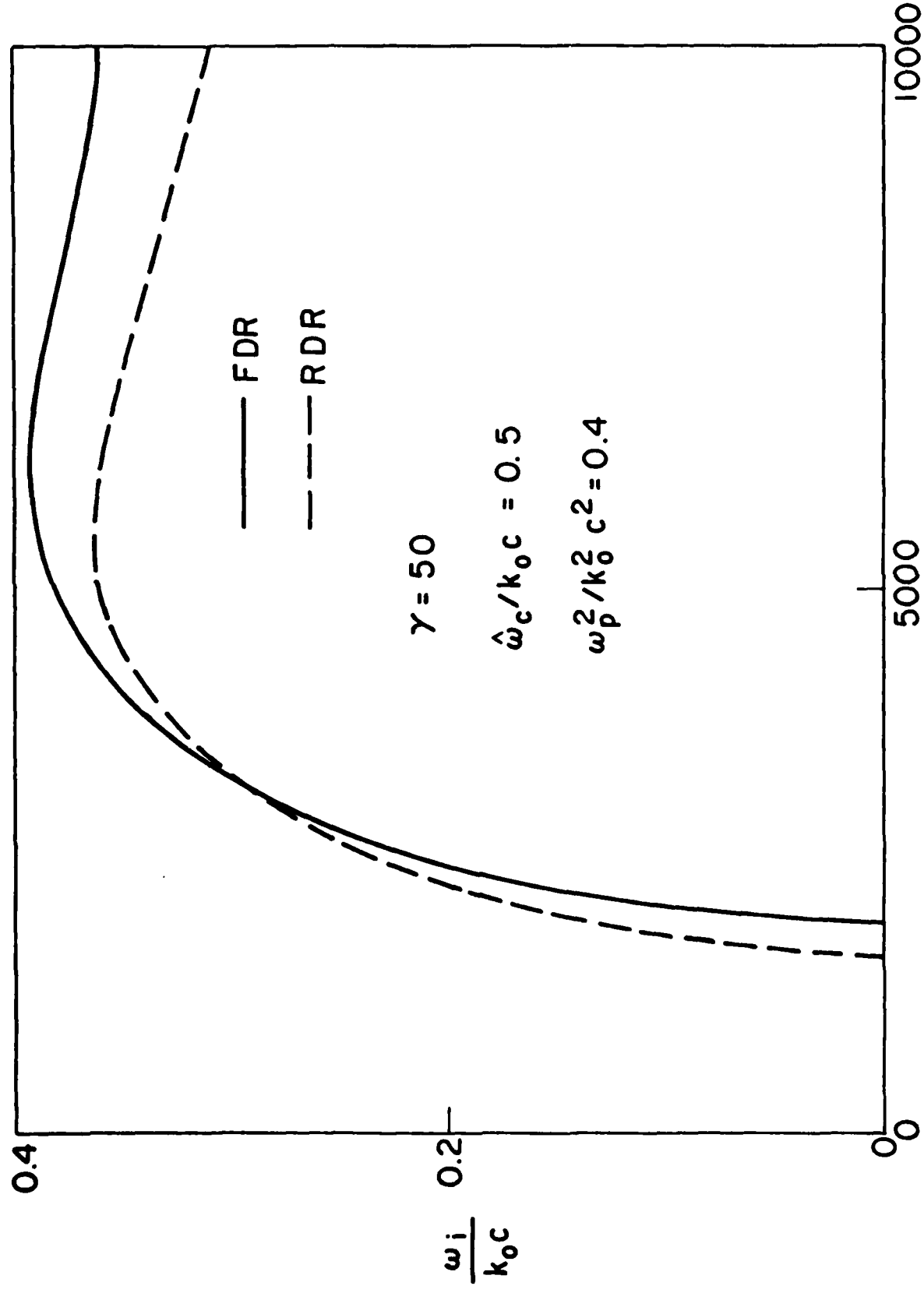
FDR
RDR
γ = 50
$\hat{\omega}_c/k_o c = 0.5$
$\omega_p^2/k_o^2 c^2 = 0.4$
0.4
0.2
0
5000
10000
$\frac{\omega_i}{k_o c}$
$(k + nk_o)/k_o$

Fig. 7

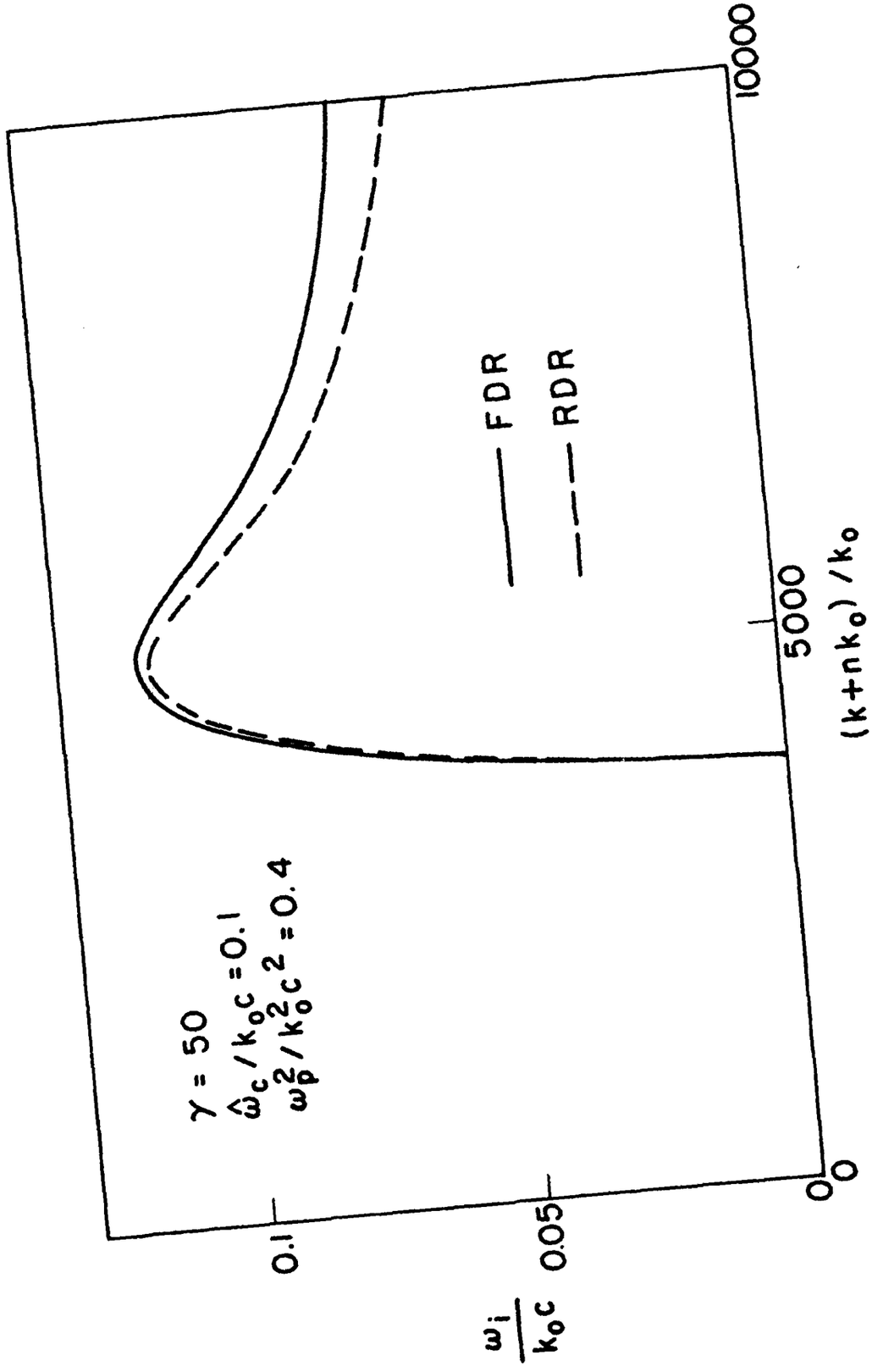
10000
5000
0
0
0.1
0.05
FDR
RDR
$\gamma = 50$
$\hat{\omega}_c / k_o c = 0.1$
$\omega_p^2 / k_o^2 c^2 = 0.4$
$(k+nk_o)/k_o$
$\frac{\omega_i}{k_o c}$

Fig. 8

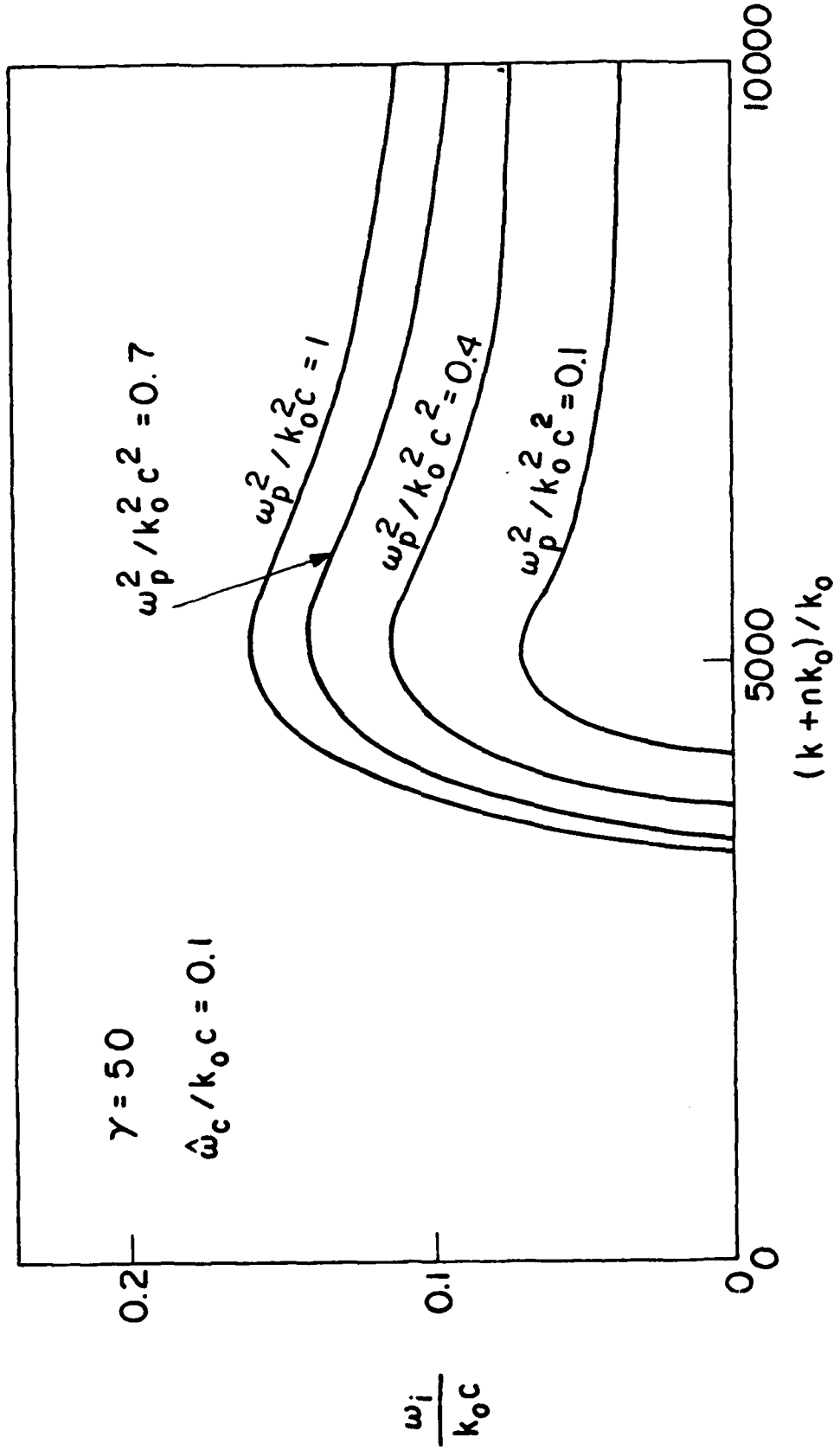
$\omega_p^2/k_o^2c^2 = 0.7$
$\omega_p^2/k_o^2c = 1$
$\omega_p^2/k_o^2c^2 = 0.4$
$\omega_p^2/k_o^2c^2 = 0.1$
$\gamma = 50$
$\hat{\omega}_c/k_oc = 0.1$
0.2
0.1
0
0
5000
10000
$(k+nk_o)/k_o$
$\frac{\omega_i}{k_oc}$

Fig. 9

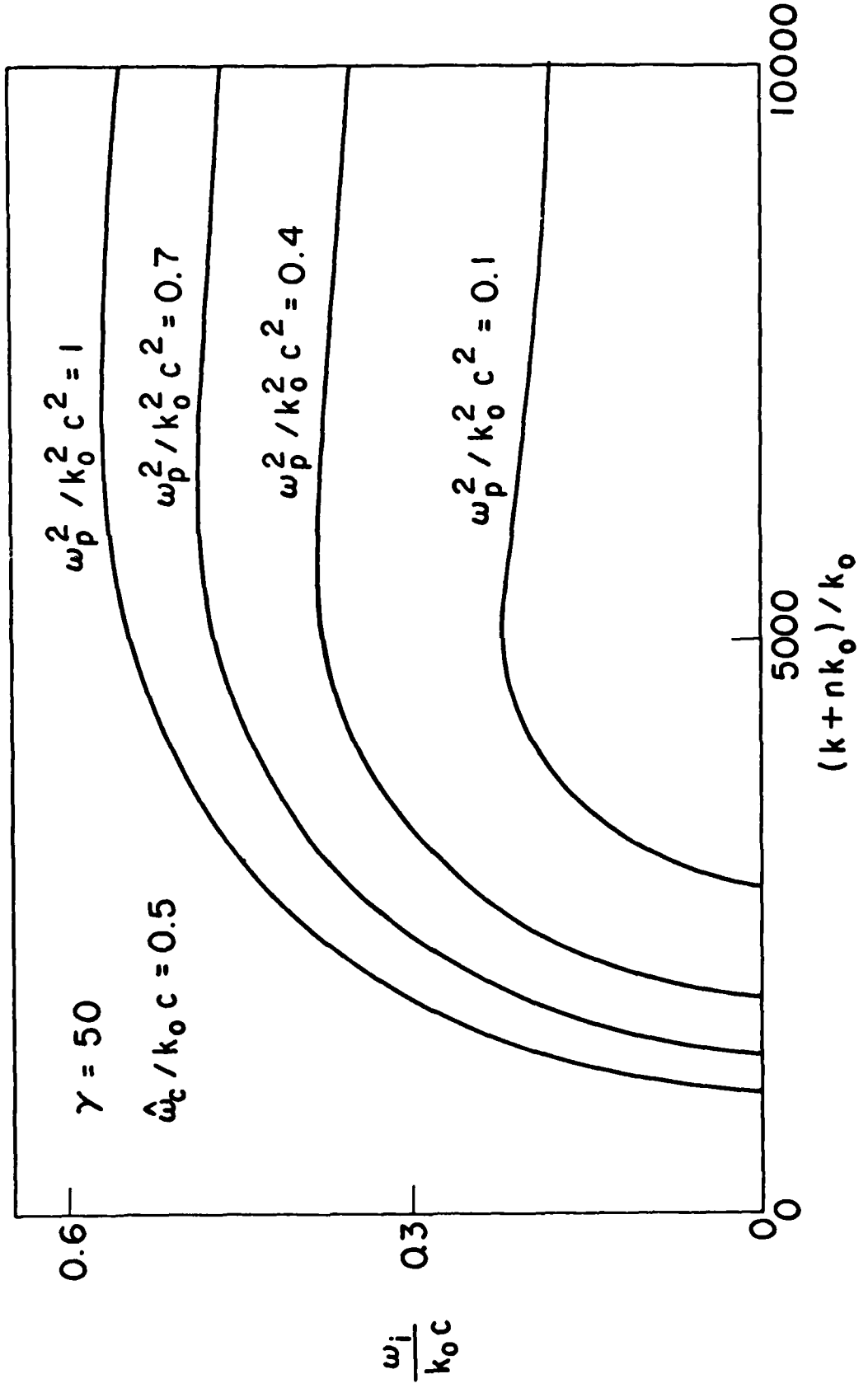
$\omega_p^2 / k_o^2 c^2 = 1$
$\omega_p^2 / k_o^2 c^2 = 0.7$
$\omega_p^2 / k_o^2 c^2 = 0.4$
$\omega_p^2 / k_o^2 c^2 = 0.1$
$\gamma = 50$
$\hat{\omega}_c / k_o c = 0.5$
0.6
0.3
0
5000
10000
$(k + n k_o) / k_o$
$\frac{\omega_i}{k_o c}$

Fig. 10

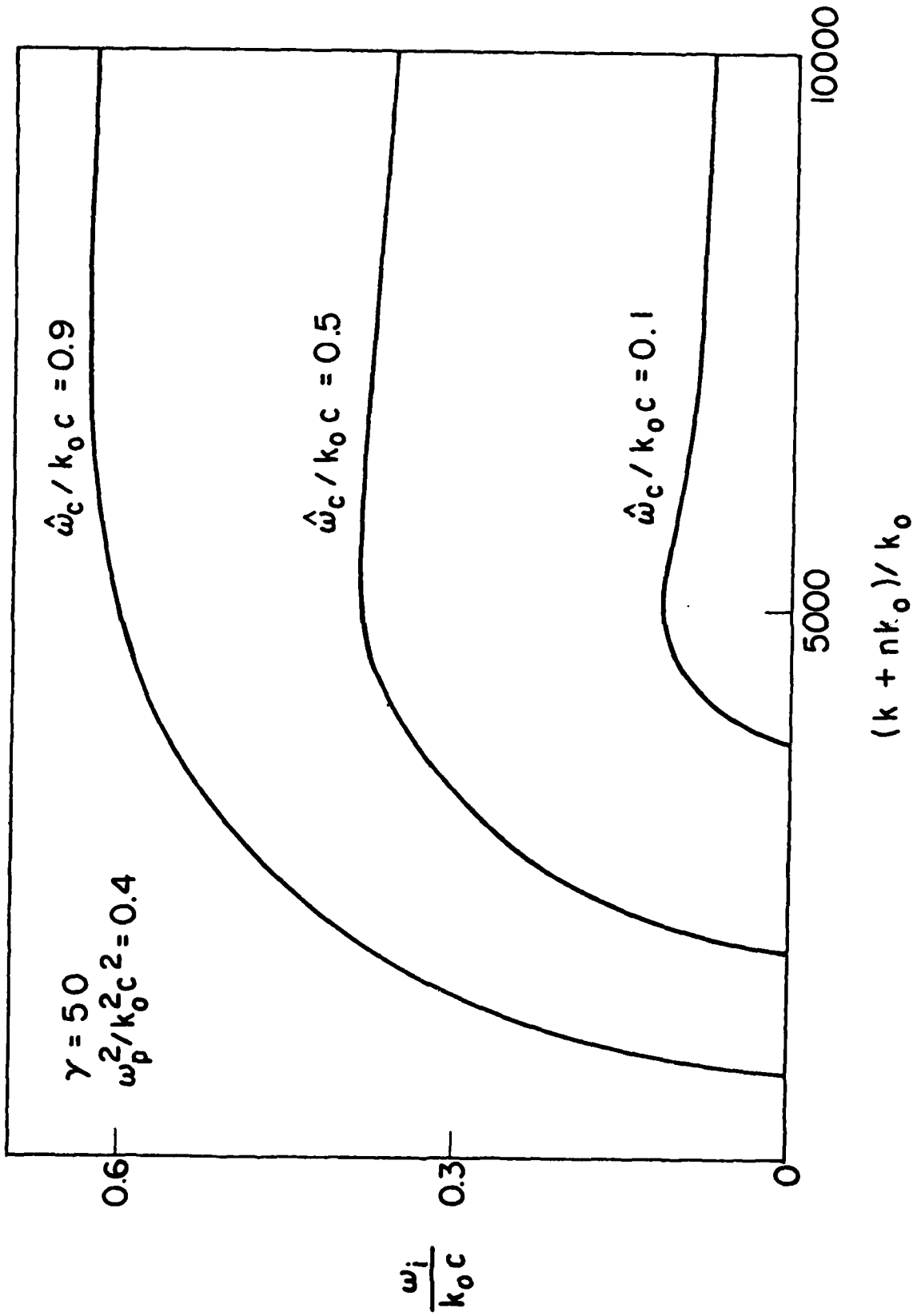
$\hat{\omega}_c / k_o c = 0.9$
$\hat{\omega}_c / k_o c = 0.5$
$\hat{\omega}_c / k_o c = 0.1$
$\gamma = 50$
$\omega_p^2 / k_o^2 c^2 = 0.4$
0.6
0.3
0
5000
10000
$(k + nk_o) / k_o$
$\frac{\omega_i}{k_o c}$

Fig. 11